A New Degenerate Fermi Gas Apparatus

by

Widagdo Setiawan

Submitted to the Department of Physics
in partial fulfillment of the requirements for the degree of
Bachelor of Science in Physics
at the

MASSACHUSETTS INSTITUTE OF TECHNOLOGY

June 2007

Author .....

Department of Physics
May 24, 2007

Certified by .....

Wolfgang Ketterle
John D. MacArthur Professor of Physics
Thesis Supervisor, Department of Physics

Accepted by .....

David E. Pritchard
Senior Thesis Coordinator, Department of Physics

A New Degenerate Fermi Gas Apparatus

by

Widagdo Setiawan

Submitted to the Department of Physics
on May 24, 2007, in partial fulfillment of the
requirements for the degree of
Bachelor of Science in Physics

Abstract

In the summer of 2004, the BEC 2 lab of Wolfgang Ketterle's group at MIT started a new research direction of studying degenerate fermionic Lithium atoms in optical lattices. The major contributions to the new experimental setup are the Lithium laser system, a new imaging technique, and an advanced experiment control system.

First, a tapered amplifier laser diode system is discussed. The laser is locked using an error signal generated using frequency modulation of saturated absorption spectroscopy of Lithium Vapor. The laser is then locked using a PID controller.

Second, a new imaging system is developed. The imaging system is designed to eliminate noise generated by the mechanical vibrations of the machine. The system relies on taking multiple images with time scale shorter than typical vibration periods.

Third, a new experiment control system is developed. The new control system replaced the outdated 8 years old control system by providing us with more channels and speed, combined with an automation feature. The new system is designed to accommodate more complex experiments in the future.

Thesis Supervisor: Wolfgang Ketterle
Title: John D. MacArthur Professor of Physics
Department of Physics

To future students of Wolfgang Ketterle's lab

Acknowledgments

Like many Indonesians who grew up on the tropical island of Bali, I never imagined I would see snow in person. That did not stop me from trying. I was lucky enough to be able to pursue my childhood dream of seeing snow and moreover, to endeavor in the world of physics. Technology in my home town was scarce, but I still wanted to work at the frontier of human knowledge. I was fortunate to be able to come to MIT where I was given the opportunity to see not only snow, but also a form of matter far more precious. For the past three years, I have been working in Wolfgang Ketterle's lab with the coldest substance in the universe: Bose-Einstein Condensates.

My personal journey as an experimentalist started when I joined Wolfgang Ketterle's lab back in the summer of 2004. Although I was only a freshman undergraduate, Wolfgang Ketterle still gave me the opportunity to join his group. Therefore, I would like to thank him for giving me a chance to learn about experimental physics from one of the best group in the world. Working in this lab has certainly taught me to become an experimentalist.

I would also like to thank Kaiwen Xu for he is the person who actually convinced Wolfgang to take me as a UROP student. During my first few months in this lab, Kaiwen taught me basic concepts of electronics and RF circuits, allowing me to learn and contribute in the lab immediately.

Jitkee Chin is always there whenever I need some advice, both for lab work and for more personal things such as graduate school. She always reminds me not to become a nerd who only cares about physics, and that there are other things than physics in this life. From time to time, she gives us leftover food from the woman in physics dinner, giving me the opportunity to enjoy good food every once in a while.

I would like to thank Daniel Miller for taking me on a ski trip for the first time in my life. Now I have accomplished a little bit more than my childhood dream of seeing snow. In the lab, Dan is the person who keeps the lab together during conflicts. When I was applying to graduate school, he gave me a lot of advice on how to revise my essays. At work, Dan is certainly the person who makes the lab lively by making stupid jokes all the time. From time to time, Dan also taught me to be able to understand jokes, a central part of American culture. Unfortunately, even to this day, I still cannot fully understand most of his jokes.

Yingmei Liu is the most hardworking person in the lab. On many occasions, she works alone until morning either to fix the machine or to take data for the experiment. Although she is a post doc, she is very easy to talk to. She is also willing to put her time into constructing electronic boxes (a job that is usually for me) that we need from time to time.

Claudiu Stan is certainly the major player in building the new Lithium setup. His experience in BEC 1 helped us upgrading our machine relatively fast. Claudiu Stan taught me a lot in producing good electronic boxes. His passion in quality taught me how to create more reliable components for the lab. Although he already graduated last year, he still helps us whenever we have problems in the lab.

Christian Sanner quickly contributed to the lab soon after he joined in early 2006. The speed of which he acquired knowledge about the lab is certainly much higher than average the graduate

students. He also brought his experience from Germany to create our lab more organized. He also routinely finds neat commercial products that we thought never existed.

Marko Cetina from Vladan Vuletic lab is an honorary member of our lab. He seems to spend more time in our lab than in his own lab. His deep knowledge in the theoretical description of feedback systems, laser diodes, imaging systems, even group theory helps us a lot routinely. He spent many days in our lab when we were setting up the new lithium laser. He taught me how to optimize the diode laser, measure the locking bandwidth, and remove the frequency noise of the laser.

Aviv Keshet brought his knowledge of waterjet cutter to the lab. He also built many electronic boxes for the lab. Using the waterjet technique, his boxes are certainly one of the prettiest. He also has a genuine interest in physics.

Tom Pasquini helped us greatly in setting up the new FM locking technique. He gave us most of the equipments required, and even spent a few days of his time teaching us on how to get the error signal.

I would also thank all other members of Wolfgang Ketterle, Vladan Vuletic, and Isaac Chuang's lab who help us whenever we have a problem. One good thing about working at MIT is that there are many people with huge amount of combined skills who are always available whenever we need help. I feel very lucky to be able to work here at MIT.

Table of Contents

Chapter 1

Introduction

1.1 Cooling and Trapping of Neutral Atoms

Our experiment revolves around creating ultracold degenerate gases. The field of ultracold degenerate gases started back in 1995 with the creation of Bose-Einstein Condensates (BEC). One technical challenge that has to be overcome in creating BEC is achieving a very low temperature. The temperature required to achieve BEC is in the order of a few microkelvin.

One limitation of using cryogenic technique to create degenerate gases is the existence of the physical contact between the gas and the container. This contact immediately transforms the gas into a solid form. To achieve ultracold degenerate gases, we have to use some other technique. One solution is to trap the atom inside a vacuum chamber without using any physical container so that we can cool the atoms without having to cool the environment.

In our setup, the experiment begins at the oven where a sample is heated to around $700\ K$. At this point, the atoms obey the Maxwell-Boltmann distribution where the atoms fly in all directions with some typical speed. Some of the atoms that have their velocity in the proper direction fly straight to the vacuum chamber.

The next step is to cool the flying atoms using a Zeeman slower. This cooling step is necessary because the traps at later stages can only confine atoms with relatively low energy (a few Kelvin). The Zeeman slower works by bombarding atoms moving in one direction by photons moving in the opposite direction. The frequency of the photons is red-detuned from the resonance frequency of the atom. The photons then excite the atoms to the excited state. Some of the atoms then decay to the ground state via spontaneous emission while emitting a photon at a random direction with an average frequency equal to the resonance frequency. Since the emitted photon energy is higher than the absorbed photon energy, the atoms lose some of their kinetic energy. If we assume that the force varies slowly over multiple scattering processes, the force is given by [1]

$$F = \hbar k \frac{\Gamma}{2} \frac{I/I_0}{1 + I/I_0 + \left[\frac{2(\delta - \boldsymbol{k}.\boldsymbol{v})}{\Gamma}\right]^2}$$

where $\hbar$ is the reduced Planck constant, k is the photon wave vector, Γ is the decay rate of the population in the excited state, I is the intensity of the laser, I_0 is the saturation intensity, $\delta \equiv \omega_{\text{laser}} - \omega_{\text{atom}}$ is the detuning of the laser frequency from the resonant frequency of the atom, and $\boldsymbol{v}$ is the velocity of the atom. This cooling method can cool the atoms to milikelvin range.

The next step is to trap and cool the atoms using the Magneto-Optical Trap (MOT) [1]. The idea is to trap the atoms using 6 laser beams from 6 different directions, combined with a magnetic field to spatially define the shape and the location of the trap. The concept of MOT is very similar to the Zeeman slower. MOT can also cool the atoms to the millikelvin range. We then trap the atoms using the magnetic trap. Since each atom has a magnetic dipole moment, the magnetic field exerts forces on the atoms. However, the magnetic trap is a conservative trap which conserves the energy of the atoms. Therefore, magnetic trap alone cannot cool the atom further. This is where evaporative cooling comes to play. Evaporative cooling works by selectively removing atoms with higher energy, leaving atoms with lower energy behind. The rest of the atoms then re-thermalize via elastic collisions. Evaporative cooling can cool the atoms to the microkelvin and nanokelvin range, which is enough to produce BEC.

Note that in the entire cooling process, we only have to cool the atoms and not the environment. The vacuum components surrounding the atoms are still at room temperature.

1.2 Ultracold Fermions

The method that we use to cool fermions is very similar to the method mentioned above. The only difference is in the evaporative cooling step. Evaporative cooling relies on the elastic collisions between atoms to re-thermalize the velocity distribution. However, the Pauli Exclusion Principle forbids collisions between identical fermions at low energy. Therefore, single species fermions cannot be cooled using evaporative cooling.

In our experiment, we cool the fermions using sympathetic cooling with bosonic atoms. The idea is to trap both bosons and fermions in a magnetic trap, and cool the bosons using evaporative cooling. Since the Pauli Exclusion Principle does not forbid collisions between different species, the fermions also thermalize with the bosons during the entire process. At the end of the process, we obtain a degenerate fermions gas.

1.3 Ultracold Fermions in Optical Lattices

Our lab specialized in studying ultracold fermions in an optical lattice experiments. The idea is to create standing waves by shining a laser beam from opposite directions, creating spatially periodic intensity variation. The laser wavelength is 1064nm which is red-detuned from the resonance frequency of the atom, which means that an atom is attracted to regions with highest intensity.

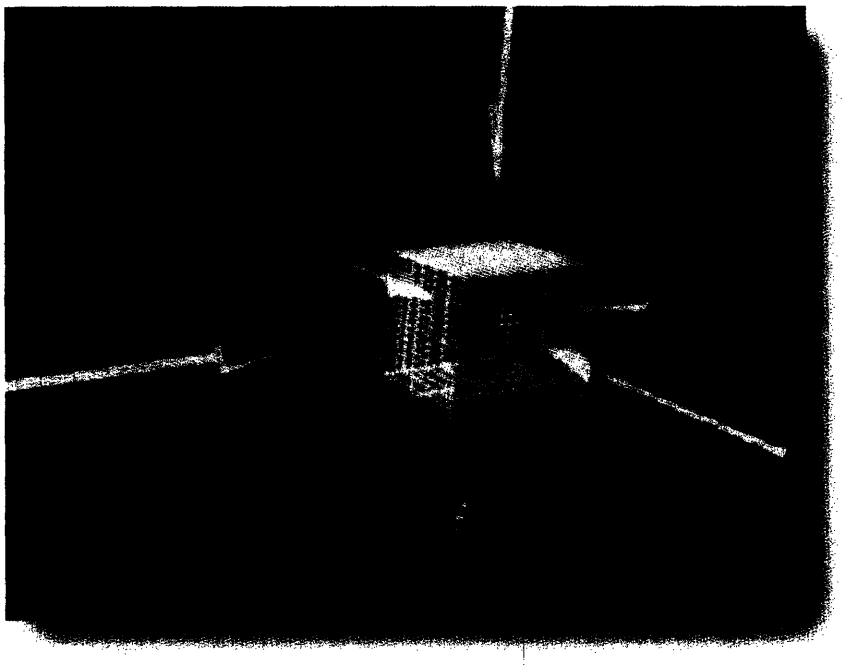

Figure 1-1. Optical lattice setup.

The typical setup can be seen in Figure 1-1. Three laser beams from three almost orthogonal directions, with three different polarizations, shine on the atoms. These beams are then retro-reflected to create standing waves which act as a 3D lattice. Note that this setup is relatively flexible. We can just turn on beams from one or two axis only, creating a 1D or a 2D lattice. Another way is to turn on beams from 2 directions with the same polarization and without retro-reflection. This will also create a 1D lattice. The advantage of this setup is that we can change the relative frequency of the two beams, creating a moving optical lattice.

1.4 Why Ultracold Fermions in Optical Lattices?

Ultracold fermions in optical lattices greatly resemble the properties of a crystalline solid. The properties of both systems are governed by interacting fermionic particles in a periodic potential, making it is possible to simulate some of the properties of a crystalline solid material using ultracold gas experiment.

One main advantage of using the ultracold gases method is the possibility of controlling the environment through a large range of possible values. We can manipulate the properties of the periodic potential such as the periodicity, the depth, and the shape of the potential by changing the optical lattice wavelength, changing laser intensity, and superimposing multiple lattices, respectively. The interaction strength between the fermions can also be modified using Feshbach resonance by simply changing the magnetic field. Furthermore, the spin states of the atoms can be prepared relatively easily in atomic physics experiments.

With these advantages, one strong motivation for studying fermions in optical lattices is to study the properties of high-temperature superconductors (high-T_c) in cuprates. The properties of this high-T_c

system are still not well understood, and understanding this system might provide practical applications such as in the development of new high-T_c superconductors.

Understanding strongly correlated fermions in optical lattices requires very complicated theoretical formulation. To simplify the problem, we have to make some approximations. If the temperature of the atoms is low enough, the system can be approximated by a Hubbard Hamiltonian [2] [3]:

$$H = -t \sum_{\{i,j\},\sigma} \left(c_{i,\sigma}^{+} c_{j,\sigma} + c_{j,\sigma}^{+} c_{i,\sigma} \right) + U \sum_{i} n_{i,\uparrow} n_{i,\downarrow} \tag{1}$$

The first term of Equation (1) represents the tunneling between adjacent sites. Here, t is the tunneling matrix element for that tunneling and $c_{i,\sigma}$ is the fermionic annihilation operator for atom in lattice site i with spin $\sigma = \{\uparrow, \downarrow\}$. The term $c_{i,\sigma}^{+} c_{j,\sigma}$ means that we annihilate the atom at lattice site j with spin σ, while at the same time creating another atom at lattice site i with the same spin σ.

The second term of Equation (1) represents the interaction energy between atoms of different spin in the same lattice site i. Here, $n_{i,\sigma} \equiv c_{i,\sigma}^{+} c_{i,\sigma}$ is the number of atoms in site i with spin σ and U is the onsite interaction parameter.

One particular system of interest is a system with repulsive interaction ($U > 0$) with a filling fraction close to 1. Unfortunately, the theoretical understanding of such a system is still very limited. It has been conjectured that d-wave pairing can exist in such a system, which might explain some of the properties of the high-T_c superconducting curprates. Creating quantum simulation of this system in ultracold gases experiments may provide some insight to this problem.

The long term goal of our experiment is to realize d-wave superfluidity. There are many techniques that still have to be developed in order to produce and detect such a state. For preliminary research toward the final goal, we have observed some evidence of superfluidity in an optical lattice via s-wave pairing [3].

1.5 Progress of the BEC 2 Lab

This section briefly describes our progress from technical points of view, especially on parts related to my projects.

When I first joined the lab three years ago on the summer of 2004, our lab did not have any fermions capability. We then decided to add fermions to the system to remain competitive in the field. The project started when we added the double species oven which was nicely designed by Claudiu Stan. The same oven has been used in BEC 1 for several years, and thus worked flawlessly in our machine on the first try.

We then had to add a suitable laser system for the lithium atoms. At first, we had some problems because the high power laser diode that was used at BEC 1 for their lithium experiment was not available anymore. Fortunately, we had a spare dye laser including two spare Argon lasers in our lab. We then installed the dye laser in our system. Unfortunately, both Argon lasers, which were used to pump the dye, gave us many problems. Some of the tens of MOSFET in the first Argon laser broke from time to time giving as a lot of down time. We then decided to change to the second Argon laser.

However, even the second laser rarely gave us enough power to run the dye laser. To be fair, both Argon lasers were already about 20 years old at the time.

After having problems with the Argon laser, we then decided to change the pump laser to a more reliable laser. One good thing about working in a big university like MIT is that there is always some spare equipment available. We borrowed a diode-pumped solid state laser called the Millennia from Vladan Vuletic and Isaac Chuang. This laser turned out to be much more reliable than the old Argon laser, giving us an easier time in running the experiment.

As good as the pump laser was, the dye laser itself is an old and complex device which requires constant maintenance. Furthermore, we only borrowed the pump laser, and we still had to return it at some point. We had to decide whether to buy a new pump laser and keep the dye laser, or change to a completely different laser system. Fortunately, starting spring 2006, a tapered amplifier diode laser for 670 nm Lithium wavelength became available. In January 2007, we replaced the dye laser with this diode laser. Chapter 2 discusses the detail of this laser. Although we had some problem for the first month, the laser has been performing very well ever since.

In early 2006, we decided to improve the imaging system. The imaging system at the time was full of noise from dust accumulated in the optical elements from the past 8 years, giving countless of interference fringes in the images. The first obvious thing that we did was to clean or replace the optical elements. Unfortunately, many of the optics were located deep inside the machine. Any cleaning operation was always associated with some risk of bumping other optical elements. The riskiest was of course cleaning the glass cell in the main chamber itself. Damaging the glass cell means rebuilding the entire vacuum chamber.

We then decided use safer methods. We first tried to clean the spatial mode of the imaging light by passing the light through an iris. This method improved the imaging quality a little bit, but it was still not enough. We also tried to use a diffuser. The idea is that spatially diffused light should not give any interference, making the light more uniform. Unfortunately, this method also failed. We finally came across a fancy double shutter camera from Cooke Corporation, which was recommended by Christian Ospelkaus from Hamburg. The camera allows us to take 2 images separated by 5 μs, enabling us to normalize most of the noise that we have in the system. The new imaging system is discussed in Chapter 3.

Doing BEC experiments requires a pretty sophisticated control system that can output a sequence of digital and analog signals reproducibly. We used software that was written back in 1999. The software had been performing very well ever since. However, there are also some problems with the software. First, we are limited to exactly 64 digital channels and 16 analog channels. This was more than enough in the past, but as the experiment grows, we were forced to multiplex a single channel to control several devices. This unnecessarily increased the complexity of the machine. Another problem is that the old software does not have any automation feature forcing us to stay in front of the computer when taking data.

I decided to rewrite a new control system for our experiment. The new software addressed both problems above, and also made some improvements on several other things. A brief overview of this new software is mentioned in Chapter 4.

There are also several appendixes describing smaller and less critical projects that I did. Appendix A describes the X Analog, the microcontroller-based universal analog device that can take

analog input and compute analog output based on the input. The device is useful for example as a very flexible PID controller. Appendix B describes the Multiscope, a computer-based 16 channel oscilloscopes. The device is useful for monitoring multiple signals from across the lab simultaneously. Appendix C describes the X Scanner, control software designed to augment the old Word Generator control software. X Scanner provides fast analog output, remote control for Agilent signal generator, and automation feature. X Scanner is the predecessor of the X Generator. Finally Appendix D describes the IPG Laser Controller, which is simple software to ramp the current of the IPG Laser in our experiment.

Of course there are a lot of other things that are required to add the lithium in our machine. However, due to lack of time, I decided to write only parts related to my projects. Other parts can be found in the PhD theses by Jitkee Chin and Daniel Miller.

Chapter 2

Laser System for Lithium Atoms

In this chapter, I will discuss the laser system that is required to slow, trap, and cool the lithium atoms. The laser of choice is a grating stabilized diode laser amplified using a tapered amplifier diode. This laser setup enables us to create a reliable laser at 670 nm with frequency stability of less than 1 MHz and power greater than 500 mW.

2.1 Basic Concept

The following discussion follows the Diploma Thesis by Martin Zwierlein [2].

2.1.1 Energy levels of Lithium

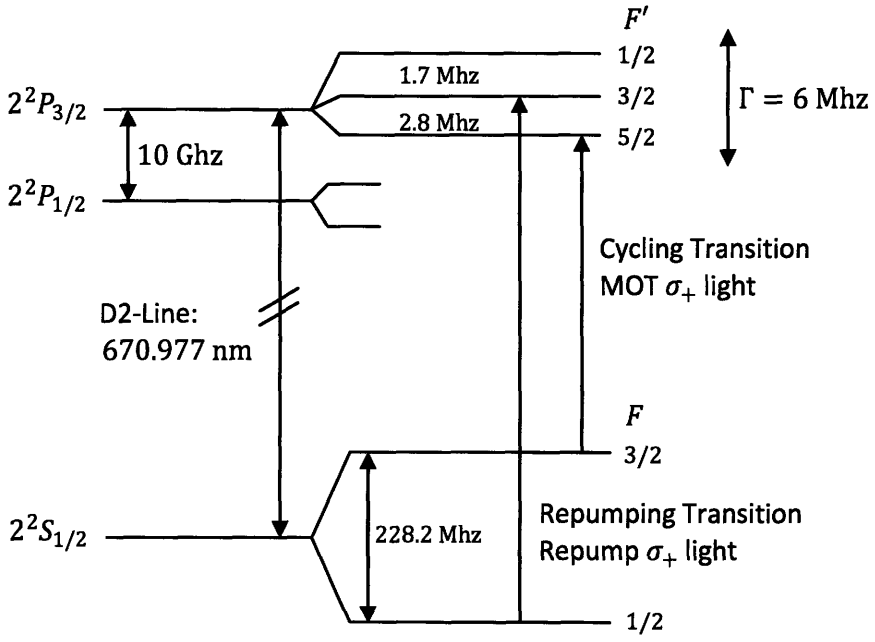

Figure 2-1. Energy levels diagram of ^{6}Li.

The lithium atom has one valence electron. Since we are interested in fermionic atoms, we choose ^{6}Li isotope for our experiment. The valence electron ground state is in the $2S$ state while the first excited

state is in the $2P$ state. The 2P state is split by fine structure splitting into $J = 1/2$ state and $J = 3/2$ state. Each of these states is then further split by hyperfine coupling. For $^6\mathrm{Li}$, the nuclear angular momentum is $I = 1$. For low magnetic fields, the states have well-defined values of $\vec{F} = \vec{I} + \vec{J}$ as shown in Figure 2-1.

One special transition in the diagram is the $F = 3/2$ ground state to the $F = 5/2$ excited state. Both of these states are the stretched state, where the angular momentum of nucleus, electron spin, and electron orbital are all aligned. Dipole transition only allows atoms in the $F = 5/2$ excited state to decay to the $F = 3/2$ ground state. This special transition is called the cycling transition. Cycling transition is desirable because the atoms are always at resonance with the laser light.

The hyperfine splitting of the excited state is smaller than the linewidth of the states themselves. Therefore, from this point on I will assume that the excited state consists only of a single state.

2.1.2 Required Lights

In order to create a Magneto Optical Trap (MOT) of lithium atoms, we need a set of laser beams with 3 different frequencies:

1. Slower Light
   Slower light is used to slow and cool hot atoms from the oven to a few Kelvin. Since the atoms are moving towards the laser beam, the laser light will appear blue shifted in the frame of the atoms. Therefore, it is necessary to red-detune the slower light such that the light will appear to be at resonance with the atoms. In our setup, we use a detuning of 540 Mhz. Furthermore, the ground state lithium atoms have 2 hyperfine states: $F = 1/2$ and $F = 3/2$ which are separated by 228 Mhz. We use an Electro-Optical Modulator (EOM) to create 10% sidebands in the slowing light. The sideband pumps atoms in the $F = 1/2$ state back to the $F = 3/2$ state. We want the atoms to be in the $F = 3/2$ state since this state, combined with σ_+ laser light, forms a cycling transition.
2. MOT Light
   The mot light is used to both spatially trap and cool the atoms. The MOT light is 20 Mhz red-detuned from the cycling transition.
3. Repump Light
   We use the repump light to pump the atoms in the MOT into the $F = 3/2$ state. The repump light is 20 Mhz red-detuned from the $F = 1/2$ transition.

2.2 Diode Laser

The laser system consists of a Master Laser and a Tapered Amplifier Laser from TOPTICA [3]. The master laser is responsible for outputting light at the correct frequency while the tapered amplifier is responsible for increasing the laser power. The diode laser system is shown in Figure 2-2. The master laser generates light at the desired frequency. The laser beam then passes through an optical isolator to prevent back reflection since a laser diode is very sensitive against back reflection. The 90/10 mirror

picks up 10% of the light that can be used for monitoring purposes. The laser is amplified in the Tapered Amplifier by a factor of 40 to 50. The amplified laser beam then passes through another optical isolator producing enough power for the entire experiment.

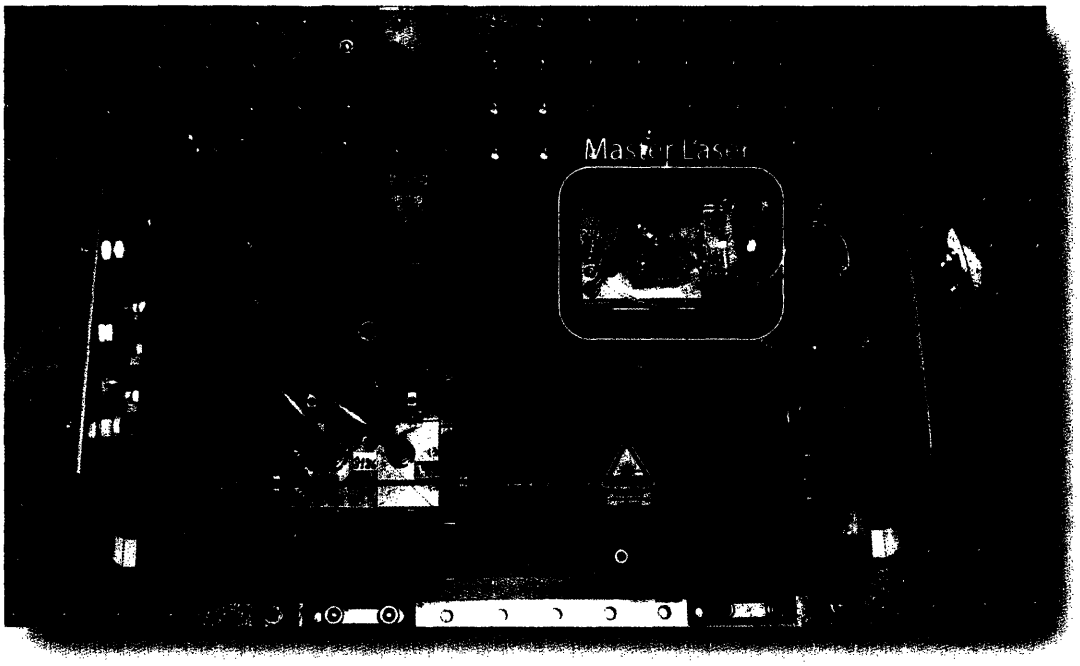

Figure 2-2. The diode laser system. The master laser generates laser light at the correct frequency. The laser is then amplified by the tapered amplifier by a factor of 40 to 50.

2.2.1 Master Laser

The master laser, shown in Figure 2-3, is a standard grating stabilized diode laser. The temperature of the laser in controlled using a single stage thermo-electric cooling (TEC) element. There is a collimation package directly in front of the diode in order to collimate the laser beam. The laser is aligned such that the 1st order diffraction of the grating is reflected back to the laser. The grating and the back facet of the diode form an external laser cavity. The front facet of the diode is AR-coated to increase the finesse of the external cavity. In order to minimize the linewidth of the laser, we want to use as many grating lines as possible. This is achieved by aligning the long elliptical axis of the spatial laser mode to be perpendicular to the laser grating. The master laser produces about 15 mW of laser power.

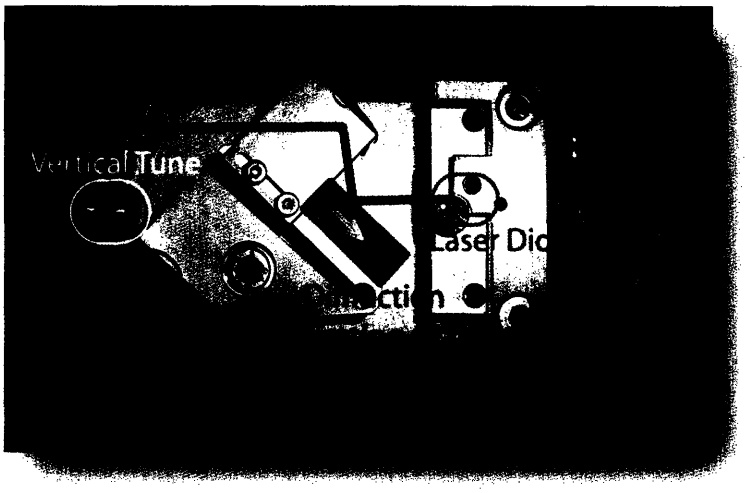

Figure 2-3. Master Laser

Grating

The grating is used to create an external cavity laser. We aligned the grating such that the first order diffraction is reflected back to the laser. The diffraction formula for the grating is given by

$$\sin\alpha = \frac{n\lambda}{2d}$$

where n is the diffraction order, λ is the wavelength of the light, d is the grating constant, and α is the diffraction angle. For the lithium light, the chosen grating constant is $d = 455\ \text{nm}$.

2.2.2 Tapered Amplifier Laser

The tapered amplifier laser is a diode laser with a small input facet in one end and a large output facet in the other end. The tapered amplifier produces a factor of 40 amplification of the laser light giving output power on the order of $530\ \text{mW}$. The tapered amplifier is located between two collimation lenses. The light from the master laser has to be mode matched to the input port of the tapered amplifier using this lens. The output of the tapered amplifier has different divergence in horizontal and vertical direction. The lens closest to the amplifier is used to collimate the high divergence component while the low divergence component is collimated using a cylindrical lens located a few cm from the tapered amplifier.

Although this lenses combination makes an almost circular beam shape, this beam still has a big amplitude and phase variation across the beam size. Furthermore, these variations also depend on the polarization of the laser as seen in Figure 2-4. In that figure, θ corresponds to the polarization angle where $\theta = 0$ is defined to be the horizontal polarization. We can see that there is a significant difference between the horizontal polarization (Figure 2-4a) and the vertical polarization (Figure 2-4b). Fortunately, 99% of the laser power is concentrated in the vertical polarization component. Otherwise, we would need a separate optical setup for each polarization.

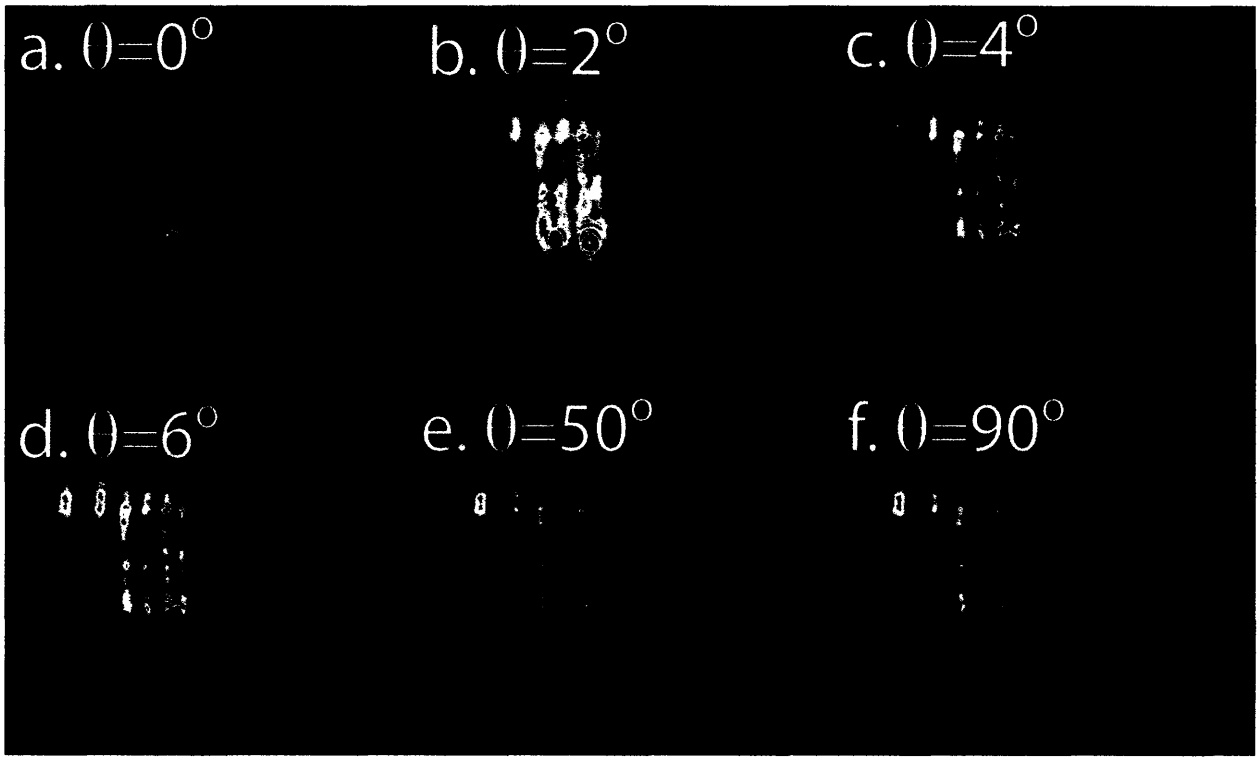

Figure 2-4. Output of the lithium laser. Figure a shows the horizontal polarization, while Figure f shows the vertical polarization. Although the interference fringes are very pronounced, the fringes actually have relatively small effect on fiber coupling efficiency. Fiber coupling efficiency of 60% is easily achievable.

We use a beam cube to separate the two polarizations. The horizontal component is used for the saturated absorption spectroscopy, while the vertical component is used for the experiment. Note that although Figure 2-4a seems to show that the horizontal component has a better beam profile (no interference), in reality the size and the shape of the horizontal component are very hard to control using a simple telescope. For this reason, we use an optical fiber to clean the spatial mode of the horizontal component before using it for saturated absorption spectroscopy.

2.3 Saturated Absorption Spectroscopy

2.3.1 Motivation

The grating stabilization above provides control of the laser frequency on the order of a few Ghz. However, since the linewidth of the Lithium transition in vacuum is in the order of 6 Mhz, we have to tune the frequency of the laser to within 2 or 3 Mhz. One simple way to tune the laser is by measuring the absorption of the laser by some lithium atoms themselves. This measurement can be used both for tuning the laser frequency to the exact lithium transition and for removing any frequency instability in the laser.

Unfortunately, measuring the laser absorption directly will not give us the precision that we need. At finite temperature, atoms or molecules in gas move at some thermal energies, which are on

the order of $k_B T$, where k_B is the Boltzmann constant, and T is the temperature of the gas. The velocity distribution along one axis is given by the Maxwellian distribution:

$$n(v_x) \propto e^{-\frac{mv_x^2}{2k_B T}}$$

where $n(v_x)$ is the number density of atoms at velocity v_x, and m is the mass of the atoms.

If we shine the atoms with laser frequency ν_0 from the $+x$ direction, the atoms will see Doppler shifted light, with Doppler shift $\Delta\nu = \frac{v_x}{c}\nu_0$, where c is the speed of light and v_x is the velocity of the atom. For 670 nm light and Lithium vapor at room temperature, the Doppler shift is on the order of 1 Ghz. This is much larger than the natural line width of the lithium atoms. Saturated absorption spectroscopy provides us a way to measure the atomic transition without the Doppler broadening effect.

2.3.2 Basic Concept of Saturated Absorption Spectroscopy

The basic idea of saturated absorption is to use a strong pump laser beam to change the velocity distribution of the atom in the ground state. The laser only interacts with one velocity group of atoms for each possible transition. The pump beam pumps the atoms at some velocity group from the ground state to the excited state. From the other direction, a probe laser beam with low intensity is shone on the atoms. For each velocity class, the Doppler shift is the opposite of the pump beam. Most of the time, the atoms will also absorb the pump beam. However, for a specific frequency of the laser, the probe beam interacts with atoms which are already pumped to the excited state. Since the probe beam effectively interacts with fewer atoms, the probe beam experiences less absorption. This only happens when both probe beam and pump beam interacts with the same atoms in some velocity group. If the probe beam and the pump beam have the same frequency, the beams will interact with atoms with velocity close to zero.

2.3.3 Saturated Absorption Spectroscopy of Lithium

Lithium has two non degenerate ground states which makes saturated absorption signals a little bit more complicated. The system has two transition frequencies. There are two cases to consider:

1. When the frequency of the laser is the same as one of the transition frequency
   This case is similar to the single transition case frequency mentioned above. The probe beam experiences less absorption since most of the atom are pumped away by the pump beam. The difference is that the atoms can be pumped both to the excited state and to the other hyperfine ground state, which makes the pumping effect a little bit stronger.
2. When the frequency of the laser is in the middle of the two transition frequencies.
   Let us assume that the pump beam interacts with the $F = 1/2$ ground state, while the probe beam interacts with the $F = 3/2$ state. Since the pump beam is strong, the pump beam will pump the atoms to the $F = 3/2$ state. Therefore, the probe beam will actually see more atoms, thus experiencing more absorption.

In the lithium case, we expect to see three peaks in the saturated absorption signal. Two of the peaks correspond to the normal transition frequencies, while the third peak should be located in between the two transition frequencies mentioned above. The third peak should also have the signal sign inverted compared to the normal transition peaks. Typical saturated absorption signal is shown in Figure 2-5.

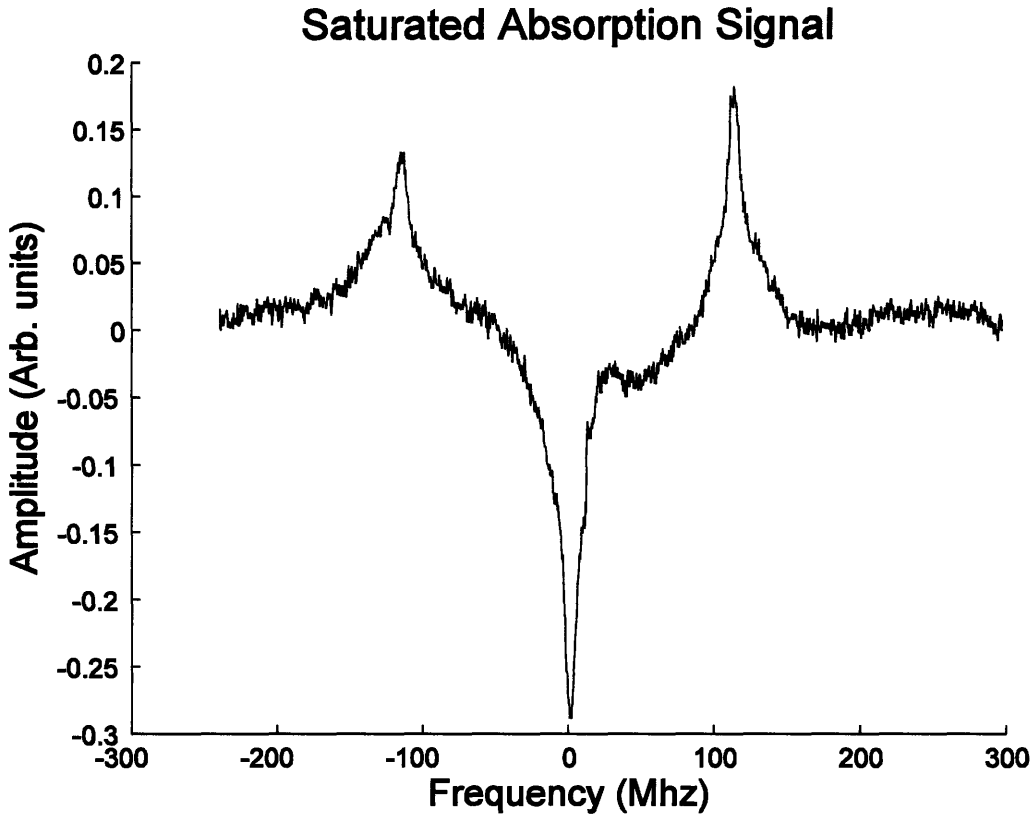

Figure 2-5. Saturated Absorption Spectroscopy of ^{6}Li. The left and right peaks correspond to the normal transition frequencies, while the middle peak corresponds to the average of the two frequencies.

2.4 Lock-In Method

2.4.1 Principle

Although the saturated absorption method enables us to measure a narrow absorption signal, we still cannot use the signal directly to lock the laser. In order to make an error signal, we need to have a zero crossing so that we know whether we should increase or decrease the frequency of the laser. One method is to take the derivative of the absorption signal so that we can lock the laser to an absorption peak which has a slope equaling to zero. The Lock-In method provides a simple way to get the derivative of the absorption signal.

The idea is to modulate the frequency of the laser beam and use heterodyne detection to measure the signal. This method measures the slope of the absorption signal directly, enabling us to use the absorption signal as the locking signal. For more information, see [2].

We used an AOM to change the frequency of the laser that passes through the Lithium vapor. We then modulate the frequency of the laser using this AOM with modulation amplitude around 10 Mhz at 100 Khz. The output signal is proportional to the derivative of the absorption signal modulated at 100 Khz. We then use an SRS locking amplifier to mix the signal with the same 100 Khz signal. The high frequency component is then removed by a low pass filter at around 1 Khz. The final output of the locking amplifier is the derivative of the locking signal itself. We then can use this signal to lock the laser.

2.4.2 Limitations

The standard lock-in method relies on the AOM to produce the frequency modulation. The inner working of the AOM relies on creating acoustic waves in the crystal. The mechanical nature of the wave makes the travelling speed of the wave relatively slow. For a typical sized AOM, it takes about 5 us for the sound wave to propagate about 1mm. Therefore, it is impossible to modulate the frequency of the AOM of this size much faster than 500 khz. Even at the maximum possible modulation frequency, the bandwidth of the error signal that we can get is still less than 50 khz. To make matters even worse, the SRS locking amplifier that we used in the past only has 1 khz bandwidth.

When we use a dye-laser system, even a 1 khz error signal bandwidth is more than enough since the dye-laser has an separate cavity locking for canceling fast fluctuation. However, the diode laser relies solely on the atomic vapor signal to stabilize its frequency. Therefore, it is necessary to lock the laser with higher bandwidth, higher than typical mechanical noise frequencies.

One way to overcome the AOM frequency limitation is by using a smaller AOM such that the travel time is significantly shorter. However, this method requires us to focus down the laser beam to a much smaller diameter. Another alternative method is to use EOM instead of AOM which is mentioned below.

2.5 FM Spectroscopy

One simple method that we can use to get a higher bandwidth error signal is FM spectroscopy. The basic idea is still the same with the lock-in method above: by modulating the frequency of the laser beam. However, we will use an Electro-Optic Modulator (EOM) instead of an AOM. Since the EOM relies on electric field, and not on acoustic waves, it is possible to modulate the frequency of the laser beam in the Megahertz or even Gigahertz regime.

2.5.1 Electro-Optic Modulator (EOM)

EOM usually consists of one or more crystals (such as Lithium Niobate) whose index of refraction changes proportionally with the electric field applied to the crystal. The index of refraction change is given by (neglecting vectorial dependence of the values) [3]:

$$\Delta n = -\frac{n_0^3}{2}(rE + sE^2),$$

where n_0 is the unperturbed index of refraction, E is the applied electric field, r is linear and s is quadratic electro-optic tensor coupling component of the crystal. For Lithium Niobate, the typical values are [4]:

$$n_0 = 2.3486$$
$$r = \frac{11.3\text{pm}}{\text{V}}$$

Assuming the crystal has length L, thickness d, and applied voltage V, the optical phase shift is given by

$$\Delta\phi = \left(\frac{\pi n_0^3 r V}{\lambda}\right)\left(\frac{L}{d}\right)$$

For typical EOM, we need voltages on the order of 200 Volts to get a π phase shift. If we power the EOM directly using 50 Ohm cable, we will need about $20 - 30$ Watt of power in order to get a reasonable phase shift. However, if we only want to drive the EOM at a single frequency, we can use a resonant circuit to boost the voltage at the EOM without using very high power amplifier.

2.5.2 Resonant Circuit for EOM

We can use a simple RLC circuit to couple and amplify RF voltage to the EOM. There are many methods to create a good resonance circuit, but one easy and effective method (taken from [5]) is to create the resonance circuit using inductor and capacitor in parallel and adding another coupling capacitor in series as show in Figure 2-6. There are 2 aspects that we should think about when designing a resonance circuit. The first aspect is the resonance frequency and the quality factor of the circuit. The second aspect is the coupling efficiency: how much of the driving power is actually delivered to the resonator.

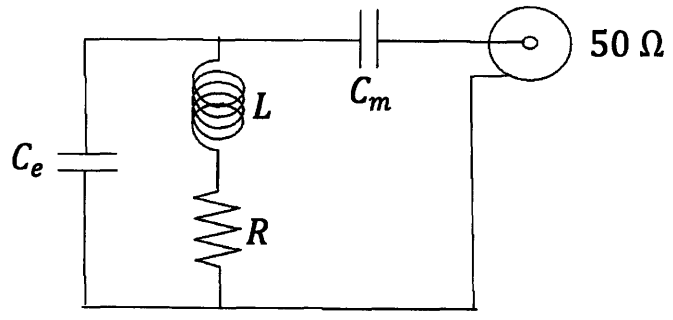

Figure 2-6 RF Resonance Circuit. C_e is the EOM parasitic capacitance (120 pF), L is an inductor, R is the parasitic resistance of the inductor, and C_m is the coupling capacitor.

We now calculate the impedance of the circuit. The following derivation follows [5]. Let us define:

$$Z_e \equiv \frac{1}{i\omega C_e}$$
$$Z_m \equiv \frac{1}{i\omega C_m}$$
$$Z_L \equiv i\omega L$$

The resonant frequency can be calculated by shorting the BNC cable, putting the 2 capacitors into a parallel configuration. Assuming that $\frac{R^2}{L^2} \ll \frac{1}{L(C_e+C_m)}$, the frequency is given by:

$$\omega = \sqrt{\frac{1}{L(C_e + C_m)}} \tag{2}$$

The total impedance of the circuit as seen by the BNC cable is given by:

$$\begin{aligned} Z = \quad & Z_m + \left[\frac{1}{Z_e} + \frac{1}{Z_L + R}\right]^{-1} = \quad Z_m + \left[i\omega C_e + \frac{1}{i\omega L + R}\right]^{-1} \\ = & \frac{1}{i\omega C_m} + \left[\frac{-\omega^2 L C_e + i\omega R C_e + 1}{i\omega L + R}\right]^{-1} = \frac{1}{i\omega C_m} + \frac{i\omega L + R}{1 + i\omega R\, C_e - \omega^2 L\, C_e} \\ = & \frac{1 + i\omega R(C_e + C_m) - \omega^2 L(C_e + C_m)}{i\omega C_m(1 + i\omega R C_e - \omega^2 L C_e)} \end{aligned} \tag{3}$$

We can now insert Equation (2) into Equation (3) to get the input impedance at the resonant frequency. The input impedance is now given by:

$$\begin{aligned} Z = & \frac{1 + iR\sqrt{\frac{C_e + C_m}{L}} - 1}{i\omega C_m(1 + i\omega R C_e - \omega^2 L C_e)} = \frac{R(C_e + C_m)}{C_m\left(1 + i\omega R C_e - \frac{C_e}{C_e + C_m}\right)} \\ = & \frac{R(C_e + C_m)^2}{C_m\left(C_m + i\omega R C_e(C_e + C_m)\right)} = \frac{R(C_e + C_m)^2}{C_m\left(C_m + iRC_e\sqrt{\frac{C_e + C_m}{L}}\right)} \end{aligned}$$

The RF amplifier and the BNC cable usually have 50 Ohm impedance. Therefore maximum coupling can be achieved when $Z = Z_0 \equiv 50$ Ohm. For simplicity, we can assume that $RC_e\sqrt{\frac{C_e+C_m}{L}} \ll C_m$. We now can solve for C_m:

$$C_m = \frac{C_e}{\sqrt{\frac{Z_0}{R} - 1}}$$

For typical values of C_e and R, we need C_m in the order of 5pF.

2.5.3 Creating Sideband Using EOM

We can use an EOM to create sidebands in a laser beam by applying sinusoidal phase modulation. Let us assume that the laser frequency is ω. The electric field of the laser measured at a fixed point in space is given by (addition with complex conjugate is implied)

$$E(t) = A\, e^{i\omega t} + \text{cc.} \tag{4}$$

Let us assume that the phase modulation is given by $\beta \sin \Omega t$. The electric field of the laser is now

$$E(t) = A\, e^{i(\omega t + \beta \sin \Omega t)}. \tag{5}$$

We can expand in terms of the Bessel function [7]:

$$E(t) = Ae^{i\omega t}\left(\Sigma_{k=0}^{\infty} \mathrm{J_k}(\beta)\mathrm{e}^{\mathrm{ik}\Omega \mathrm{t}} + \Sigma_{k=0}^{\infty} (-1)^{\mathrm{k}}\mathrm{J_k}(\beta)\mathrm{e}^{-\mathrm{ik}\Omega \mathrm{t}}\right).$$

If $\beta \ll 1$, we can expand the exponent:

$$\begin{aligned} E(t) &= Ae^{i\omega t}\, e^{i\beta \sin \Omega \mathrm{t}} \\ &= Ae^{i\omega t}\,(1 + i\beta \sin \Omega t + \cdots) \\ &\approx A\left(e^{i\omega t} + \frac{\beta}{2} e^{i(\omega+\Omega)t} - \frac{\beta}{2} e^{i(\omega-\Omega)t}\right) \end{aligned} \tag{6}$$

The last line shows that the light now consists of the primary light accompanied by 2 sidebands with amplitude $\frac{\beta}{2}$.

2.5.4 Effect of Absorption on Light

We now send this light to the atomic vapor cell. We also send the pump beam from the other direction (without any sideband) so that we can observe the Doppler free signal. The following derivation follows from [6]. Let us define the transmission coefficient:

$$T_n = e^{-\delta_n} e^{-i\phi_n},$$

Where δ_n and ϕ_n are defined to be real and positive. δ_n represents the absorption of the n^{th} sideband and ϕ_n represents the phase shift due to the dispersive feature of the absorption. Here I associate $n = -1,0,1$ light with frequency $\omega - \Omega, \omega, \omega + \Omega$ respectively. Inserting this equation into Equation (6), we get

$$E(t) = A\left(T_0 e^{i\omega t} + \frac{T_1\beta}{2} e^{i(\omega+\Omega)t} - \frac{T_{-1}\beta}{2} e^{i(\omega-\Omega)t}\right) + \text{cc.}$$

We then measure this light in a fast photodiode. The photodiode can only measure the intensity, not the amplitude, of the light, which is proportional to $I(t) \propto E^2(t)$. From now on, I will assume the proportionality constant to be 1. The intensity will consist of terms from DC to terms that are proportional to 2ω. Since the photodiode can only measure relatively slow oscillation, I will neglect the terms faster than ω and terms in the order of β^2. The intensity is given by:

$$I(t) = A^2 e^{-2\delta_0} \begin{pmatrix} + & 1 \\ +\beta\cos\Omega t & \left[e^{\delta_0-\delta_1}\cos(\phi_0-\phi_1) - e^{\delta_0-\delta_{-1}}\cos(\phi_0-\phi_{-1})\right] \\ -\beta\sin\Omega t & \left[e^{\delta_0-\delta_1}\sin(\phi_0-\phi_1) + e^{\delta_0-\delta_{-1}}\sin(\phi_0-\phi_{-1})\right] \end{pmatrix}$$

It is useful to make an approximation where the frequency of the sideband is in the same order as the size of the absorption signal, that is $|\delta_m - \delta_n|\text{and}|\phi_m - \phi_n| \ll 1$. Using this approximation we get

$$I(t) = A^2 e^{-2\delta_0} \begin{pmatrix} + & 1 \\ +\beta\cos\Omega t & [\delta_{-1} - \delta_1] \\ -\beta\sin\Omega t & [2\phi_0 - \phi_1 - \phi_{-1}] \end{pmatrix} \tag{7}$$

The intensity signal consists of 3 parts:

1. The constant term which is proportional to the absorption in the vapor cell
2. The term modulated by $\cos\Omega t$
   This term measures the difference of the absorption of the right sideband to the left sideband. The signal can be thought as the derivative of the absorption signal.
3. The term modulated by $\sin\Omega t$
   This term measures the second derivative of the dispersion curve of the absorption signal.

Using the heterodyne detection method, we can choose which of the three components to observe. For our purpose, we take the second term, which is the term proportional to the derivative of the error signal.

2.6 Locking the Laser

In order to use the laser for atomic physics experiments, we have to control the frequency of the laser to within 1 Mhz. We use active feedback to control the frequency of the laser.

A diode laser is very sensitive against vibration. We can easily change the frequency of the laser simply by talking close to the laser. Since the lab inherently produces a lot of noise from fans of power supplies, laser shutter, servo motors, air filter fans, and other things, removing all of these noises is impractical. Fortunately, mechanical vibration usually is limited to a maximum frequency of around 10 khz. We can solve mechanical noise problem simply by locking the laser with around 10 khz bandwidth or higher.

2.6.1 Locking Setup

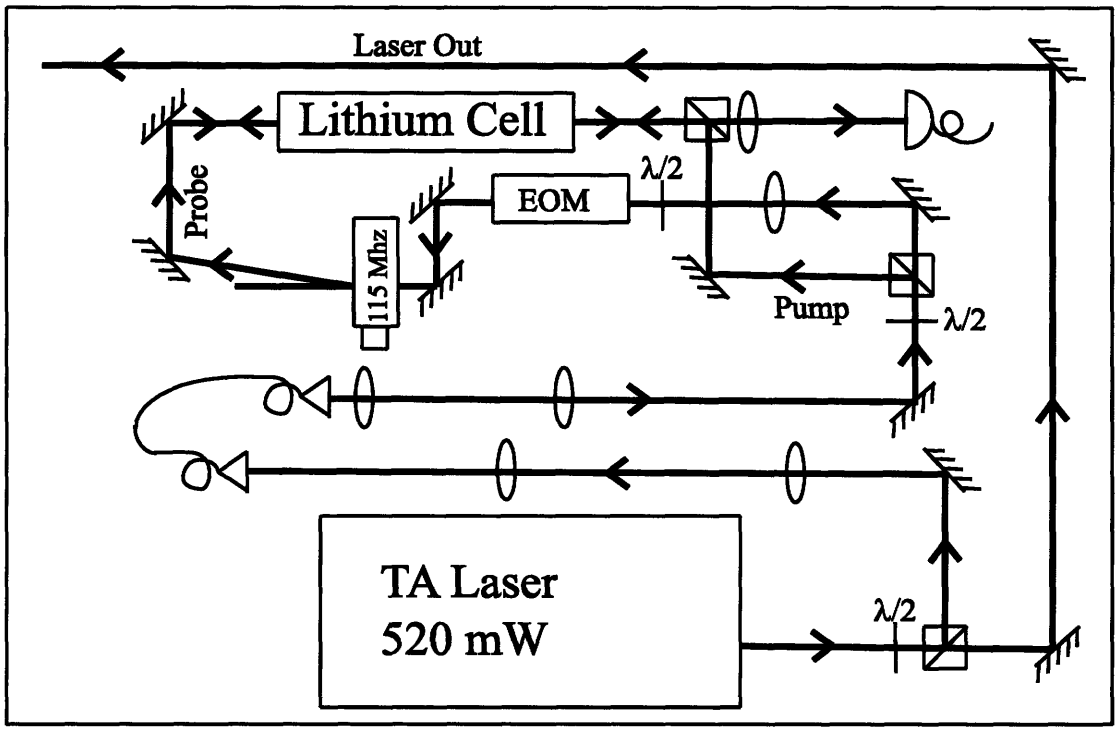

Figure 2-7. Experimental Setup for Saturated Absorption Spectroscopy.

The locking setup for the Lithium laser is shown in Figure 2-7. We first couple 5 mW out of the laser using a polarizing beam splitter. It turns out that the horizontal polarization of the laser has a very bad spatial mode, so the beam cube also separates the good spatial mode and the bad spatial mode of the beam. We are using the bad spatial mode for locking purposes so that the good spatial mode can be used solely for the experiment. We first clean this beam by passing the beam through a single mode optical fiber. We then split the beam into the pump beam and the probe beam with equal power. We then put 35 Mhz sidebands on the probe beam. We also shift the frequency of the probe beam by 115 Mhz. We then align both beams such that they overlap with each other inside the lithium cell. Finally, we detect the absorption signal in the photodiode. Since the frequency modulation is 35 Mhz, the bandwidth of the photodiode must be at least 35 Mhz.

2.6.2 Error Signal

This locking setup uses both the saturated absorption spectroscopy effect and the FM modulation effect mentioned in Section 2.5.4 above. We are interested in the second term of the signal, (see Equation (7)) which is proportional to the derivative of the absorption signal.

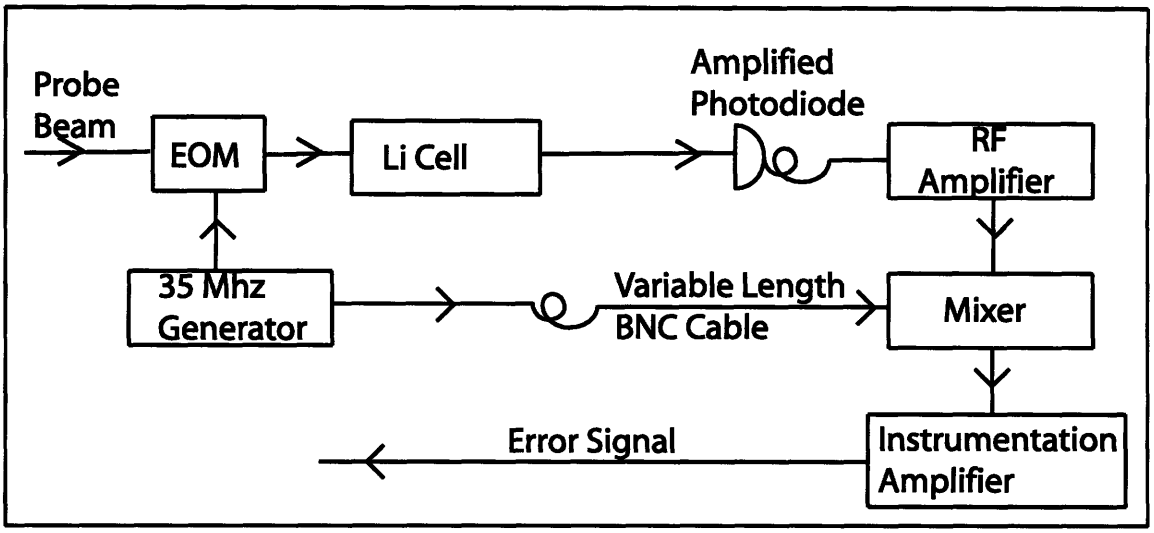

Figure 2-8. Error signal generation.

We have to use some RF electronics, as shown in Figure 2-8, in order to get the desired signal. The signal from the photodiode is given by Equation (7). The RF amplifier then amplifies the signal from the photodiode. The amplifier also acts as a high pass filter, removing the first term of Equation (7). We then mix the signal with the 35 Mhz signal. We have to adjust the length of the BNC cable such that we only pick up the second term of Equation (7). We then use an instrumentation amplifier to amplify this signal. The instrumentation amplifier also acts as a low pass filter, removing the 70 Mhz component in the signal. The output of the instrumentation amplifier can be used as an error signal. Typical error signal is shown in Figure 2-9.

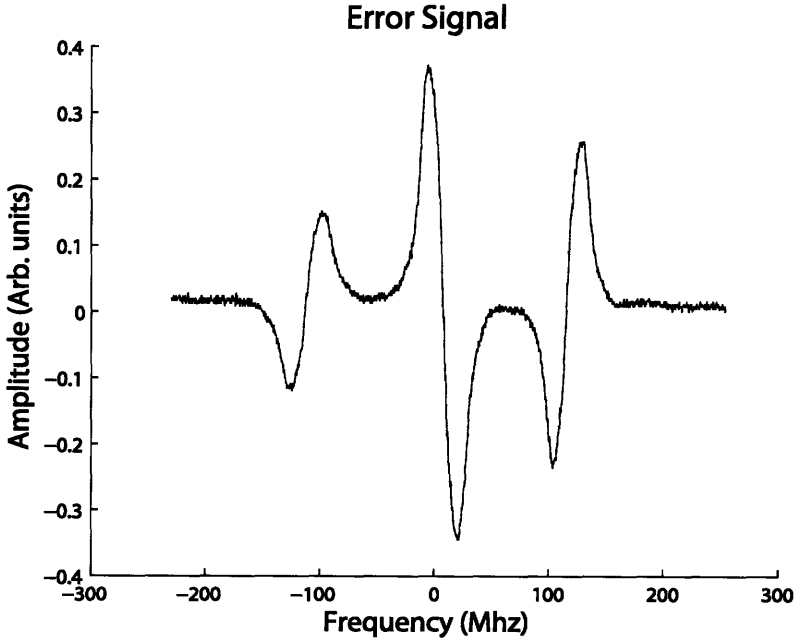

Figure 2-9. Typical error signal.

2.6.3 External Control Ports of the Laser

The Tapered Amplifier system from Toptica has 4 different input ports for external frequency feedback. These inputs are:

1. External piezo control.
   This input accepts a control voltage signal that in turn will change the voltage offset of the piezo, which controls the grating angle of the master laser. There is also a potentiometer in this piezo control that is used to feed forward the voltage signal to the current control. The piezo itself has resonant frequencies at 2 khz and 10 khz. This bandwidth limitation makes this input unsuitable for frequency locking except for low frequency drift.
2. External current control.
   This input also accepts a voltage input that in turn will control the current through the laser diode. In order to protect the laser, this input is internally filtered using a second order low pass filter at around 15 khz. This input is fast enough to cancel all mechanical noise in the laser.
3. Mosfet current bypass control.
   If we need to lock the laser with higher bandwidth, we can control the mosfet, which is attached in parallel with the laser diode itself. This input has around 5 Mhz bandwidth.
4. Current bias control.
   This input accepts a current that will be fed directly to the laser diode. Since this input is directly connected to the laser diode, this input should only be used with extreme caution and only after testing the driving circuitry extensively. This input has around 20 Mhz bandwidth which is useful when we need to phase-lock the laser.

2.7 Locking Performance

Currently, we lock the laser using the second port, (external current control) giving us a locking bandwidth of around10 khz. This setup has been used for the past 4 months without any problems.

Chapter 3

Imaging System

In BEC experiments, data is taken by capturing absorption images of the atomic cloud. This is done using a resonant laser beam such that the atoms absorb some of the incident light. A CCD camera then captures the image.

The imaging procedure consists of taking an image of the probe light with the atoms, an image of the probe light without the atoms, and an image without any probe light (just capturing the background light level). We then subtract the third image from the first and second image to remove the background light level. Finally, we divide the first image with the second image to get the normalized absorption signal.

3.1 Overview of CCD Camera

A CCD camera consists of many light-sensitive capacitors, aligned in a grid pattern. The capacitors collect charges that are produced by the photo-electric effect. A typical CCD camera has a quantum efficiency above 50%. One essential feature of any CCD chip is the capability of transferring electric charges from one pixel to another with very little loss. At the end of the chip is an analog to digital converter that converts the charges into digital signal. This signal is then transferred to the computer for further processing.

3.1.1 Typical parameters of CCD Camera

There are several parameters that should be considered when choosing a CCD Camera:

1. Readout Noise
   This is the noise of the analog to digital converter (ADC) in the CCD camera when reading the signal from each pixel. The typical noise is in the order of 7 electrons.
2. Readout Resolution
   The ADC usually has a readout resolution of 12 bit or 16 bit. This limits the maximum contrast that can be recorded by the CCD camera.
3. Readout time
   It takes the ADC some time to be able to read every single pixel in the camera. The typical readout time is on the order of several hundred milli seconds.
4. Dark Current

Since the temperature of the camera is finite (non zero), there is a probability that thermal excitation will excite electrons in the capacitors. Some CCD cameras are cooled in order to reduce this noise. At room temperature this noise is on the order of 1 electron/second for each pixel. In a BEC experiment, we are usually only limited by the readout time of the ADC which is in the order of 100 ms. This readout time produces dark noise of less than one electron. Therefore, dark current is usually not relevant in a BEC experiment.

5. Quantum Efficiency
   Depending on the wavelength, CCD chips can usually capture more than 50% of the photons received.
6. Well Capacity
   The capacitors can only store certain amount of charges which is usually on the order of a few hundred thousand electrons. If we put more charges, the capacitor charge will leak and we will not be able to read the excess signal. There is also a possibility for the charges to leak into other capacitor wells which is called blooming.

3.1.2 Interline CCD Camera

Commercial cameras usually use Interline CCD chips to eliminate the need for a mechanical shutter in the camera. The working principle of interline CCD chip is shown in Figure 3-1 a-d. The idea is to create 2 kinds of pixels in the CCD, bright pixels and dark pixels. Bright pixels are exposed directly to light that get into the camera at all time, while the dark pixels are covered such that they never receive any light. These pixels are arranged in lines inside the CCD chip such that each bright pixel has a corresponding dark pixel—thus the name interline CCD camera. When a user triggers the camera to take an image, the camera shifts the electrons in each bright pixel to the corresponding dark pixel. This makes the bright pixels empty and ready to record any incoming photon. At the same time, the camera cleans the electrons from all dark pixels. Once the desired exposure time is reached, the camera shifts the bright pixel to the dark pixel once more. Now the dark pixels store the image that is taken. Since the dark pixels never receive any light, the camera can slowly read the signal from the dark pixels and store the image in the camera memory (or transfer the image to the computer). This enables the camera to take a picture without any mechanical shutter. This feature is also called the electronic shutter.

3.1.3 Double Shutter CCD Camera

A double shutter camera also uses an interline CCD chip. Different from the standard interline camera which only reads one image per trigger event, a double shutter camera also reads the second image which is captured while the first image is being read as shown in Figure 3-1 a-g. This enables the camera to take 2 images with very short time interval because the camera does not have to wait for the time it takes to read the first image before capturing the second image. However, the exposure of the second image is determined solely by the readout time of the first image since we cannot transfer the second image to the dark pixels while the camera is still reading the first image.

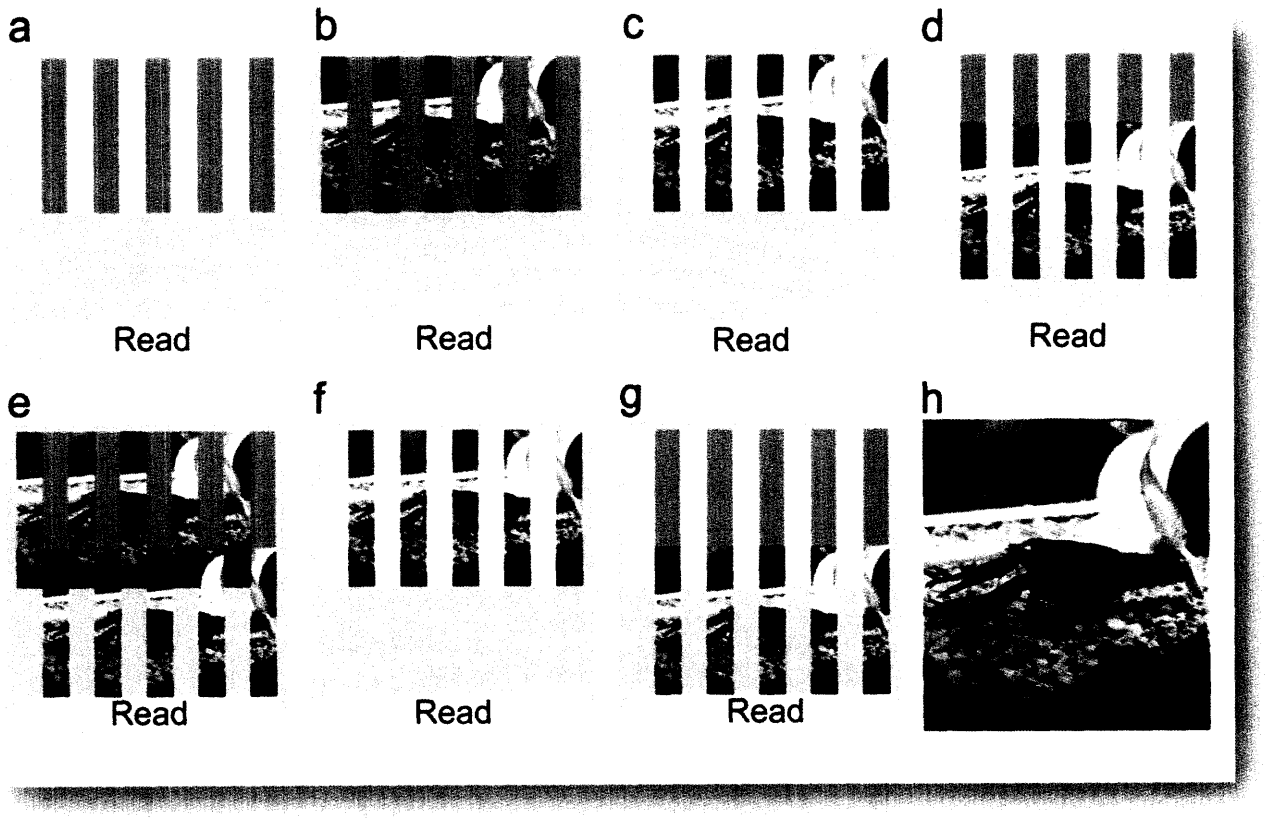

Figure 3-1. Working principle of an Interline and Double Shutter Camera. Figure a shows how the CCD chip consists of dark and bright stripes. The dark part cannot receive any photon from outside while the bright part receives photons from outside the camera all the time. Figure b shows how the bright part captures the photons from outside. Figure c shows how the image is transferred to the dark part. Figure d shows how the camera reads the image from the dark part. Interline camera finishes the data taking procedure after step d. However, a Double Shutter Camera has several extra steps. Figure e shows that while the image in the dark part is being read, the bright part can record another image. Figure f and g shows that the second image is transferred to the dark part and read by the camera.

In our experiment, the Double Shutter Camera is a Pixelfly QE camera from PCO Imaging [8] shown in Figure 3-2.

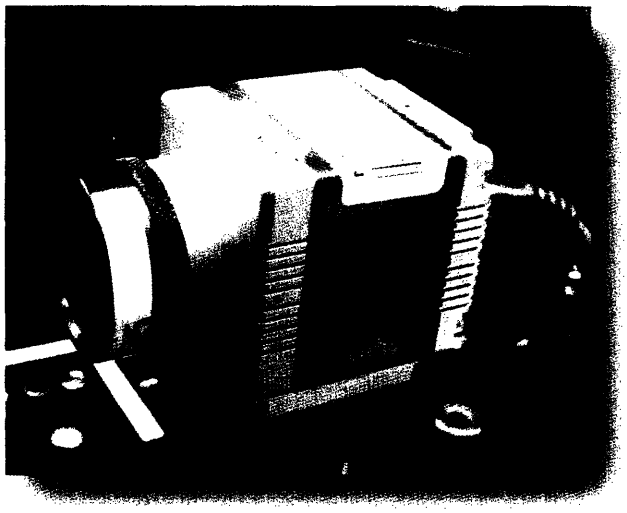

Figure 3-2. Pixelfly QE Double Shutter Camera from PCO Imaging.

3.2 Old Imaging System – Full Frame Camera

In order to image the atoms, we shine a resonant laser beam onto the atomic cloud. The atoms in turn absorb part of this light, leaving a shadow behind. We use lenses such that the camera can image this shadow created by the atoms.

Unfortunately, the dust accumulated in the glass cell makes this laser beam non uniform. This makes the shadow image of the atom polluted with interference fringes. Sample image is shown in Figure 3-3. Another imperfection that has to be considered is the stray light that is collected by the camera, especially for a camera without shutter.

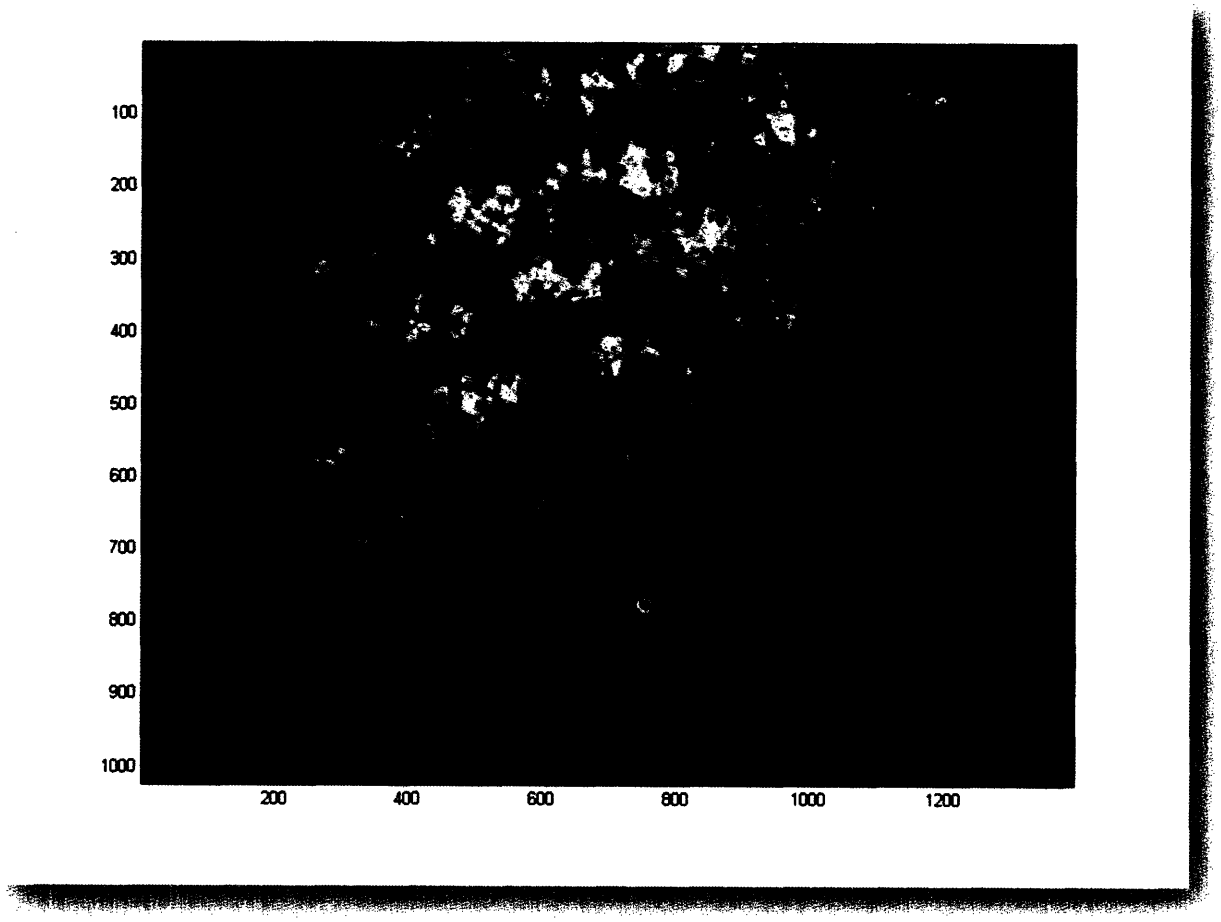

Figure 3-3. A sample raw image from the imaging axis. The BEC can be (barely) seen in location (790,620).

The stray light problem can easily be solved by subtracting the image with a reference background image which is taken without shining any laser light. In order to eliminate the non-uniformity, we can normalize the image with another image taken without any atom. The images required for this procedure are:

1. Image with probe light and atoms
2. Image with probe light without atoms
3. Image without probe light

The final image is

$$I_{final} = \frac{I_1 - I_3}{I_2 - I_3}$$

This method cancels both the stray light and non-uniformity problem in the imaging system.

3.2.1 Problems with the Old Imaging System

Although in principle, the normalization procedure above should eliminate the interference fringes in the camera, the vibration of the system makes the normalization imperfect. The location of the interference fringes taken in the first and second shots differ a little bit (sub pixel) because the dust in the optics moves with the optical elements as a function of time due to mechanical vibration.

The primary source of the imperfect normalization is the vibration is in the glass cell. The vibrations of the glass cell are excited by the magnetic trapping coils surrounding the glass cell. In turn, the magnetic coil vibration is generated by the Lorentz force whenever we change the current in the coil abruptly.

3.3 New Imaging System - Interline/Double Shutter Camera

The new imaging system is designed to solve the imperfect normalization problem above. The new double shutter camera has a different image normalization procedure:

1. Image with probe light and atoms – short exposure
2. Image with probe light without atoms – long exposure
3. Dark field 1 - Image without probe light – short exposure
4. Dark field 2 - Image without probe light – long exposure

The first image is usually taken with about 40 μs exposure time. The double shutter camera does not allow the user to control the exposure time of the second image. The exposure time is limited by the readout time of the camera which is about 100 ms / image. This makes the stray light field of the first image differs considerably (because of 1000 times more exposure time) from the second image. Therefore, it is necessary to take two dark field images, one with the short exposure, and one with the long exposure to cancel the respective stray light field. In this setup, we essentially take 2 pairs of images. The final image is given by :

$$I_f = \frac{I_1 - I_3}{I_2 - I_4}$$

3.3.1 Hardware - Pixelfly QE Double Shutter Camera

This section discusses the basic differences between the new Pixelfly Double Shutter Camera, and the Princeton Instruments Pixis 1024 Camera (our old camera). The basic differences are shown in Table 1.

	Princeton Instruments – Pixis 1024	Pixelfly QE Double Shutter
QE	80%	50%
Pixel Size	13 μm x 13 μm	6.5 μm x 6.5 μm
Temperature	-75^oC, TEC and water cooled	50^oC, no cooling
Readout Noise	9 e^- rms (fast mode)	8 e^- rms
Readout Time	580 ms (fast mode)	$\approx$ 100 ms
Dark Current	0.02 e/pixel/second	1 e/pixel/second
Readout Resolution	16 bit	12 bit

Shutter	Yes	No
Size	Big	Small
Inter-framing time	600 ms	5 μs

Table 1. Princeton Instruments – Pixis 1024 vs Pixelfly QE Double Shutter Comparison Table.

The primary feature that we are looking for in the Pixelfly camera is of course the $5\mu s$ inter-framing time. However, using the Pixelfly camera comes at a cost. The quantum efficiency is considerably lower than the Princeton Instruments camera, which effectively increases the noise in the imaging system. Depending on the application, this trade-off can be acceptable or unacceptable.

3.3.2 Software

The Pixelfly Double Shutter Camera comes with a bundle of software for many different applications starting from Photoshop, Matlab, Labview, and plain DLL library. I choose to control the camera using Microsoft C# programming language for the flexibilities offered by the language. The software interacts with the camera using the provided DLL library.

3.3.3 Improvement

The improvement that we get by using this new imaging technique was beyond expectation. Before we used the camera, we tried many different methods to clean our imaging system for example by cleaning or changing the optical elements, putting a diffuser to reduce the interference, use an iris to spatially filter the spatial mode, and use the frame transfer feature in the old camera to reduce the inter-framing time. Combining all of those methods only improved the imaging quality marginally. Note that the frame transfer method also fails because the minimum inter-framing time is still on the order of a few ms, slower than the vibration frequency.

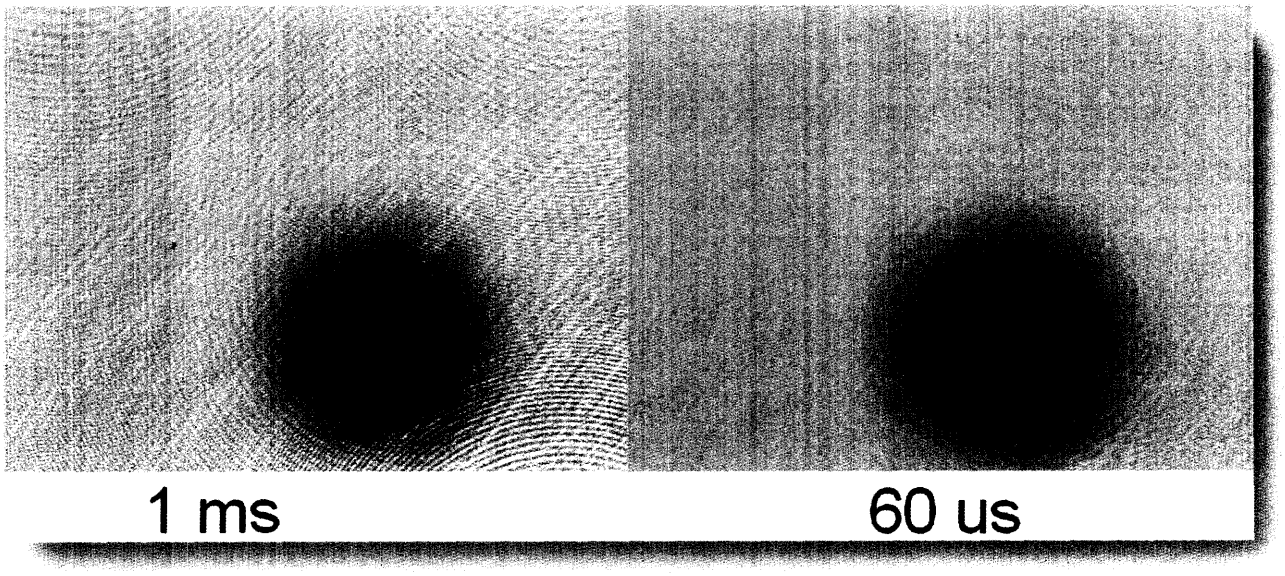

Figure 3-4. Improvement of the imaging system by simply decreasing the time between shots. The left images is taken using 1ms inter-framing time, while the right image is taken using 60 μs inter-framing time.

The improvement of the new imaging system can be seen in Figure 3-4. Both images are taken using the new imaging system. The only difference is the time between the two shots (probe light with atoms and probe light without atoms). We can see the most of the interference fringes disappear once we lower the inter-framing time to 60 μs.

3.4 Vibration Frequency Measurement

Since the new imaging system can operate in tens of micro seconds regime, we can measure the mechanical vibration frequency of the machine which is in the order of 10 Khz.

3.4.1 Experimental Setup

The experimental setup for the vibration measurement is shown in Figure 3-5. We simply shine a laser light through the glass cell and observe the interference fringes produced at the camera. We use the Double Shutter feature to record two flashes of light separated by a few tens of micro seconds. The internal vibration of the glass cell shifts the location of the interference fringes in the 2 shots.

Figure 3-5. Simplified experimental setup for the vibration measurement. Coherent laser light shines through the glass cell. The glass cell attenuates the laser non-uniformly causing interference fringes. The light is then measured by the CCD Camera.

We measure the oscillation frequency of the glass cell using this method. The time sequence is shown in Figure 3-6. Initially, the magnetic coil is turned off abruptly producing some amount of force in the system. The glass cell absorbs some of the energy and transforms the energy into vibration. We then wait for about 1 ms such that only high Q oscillations remain. We take 2 images separated by Δt which is on the order of a few tens of micro seconds. Finally, we plot the amplitude of the interference fringes as a function of Δt. By measuring the periods of the amplitude oscillation, we can determine the oscillation frequency of the glass cell.

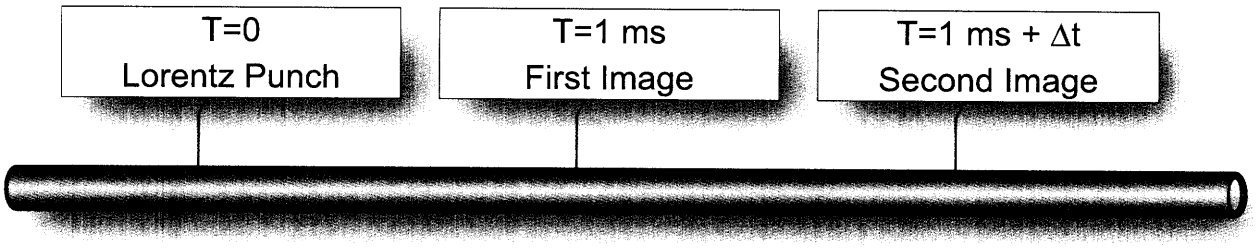

Figure 3-6. Time sequence for frequency measurement. We initiate the vibration by turning the magnetic field off abruptly at $T = 0$. We then wait for 1 ms for the low Q oscillation to decay. We then image twice with variable time in between to measure the interference fringes.

Result

The result of the glass cell frequency measurement is shown in Figure 3-7. Δt is scanned from $50\ \mu s$ to $380\ \mu s$. The amplitude of the interference fringes is plotted as a function of Δt. The measured oscillation frequency is about 6 khz. This frequency most likely corresponds to the internal vibration of the glass cell itself.

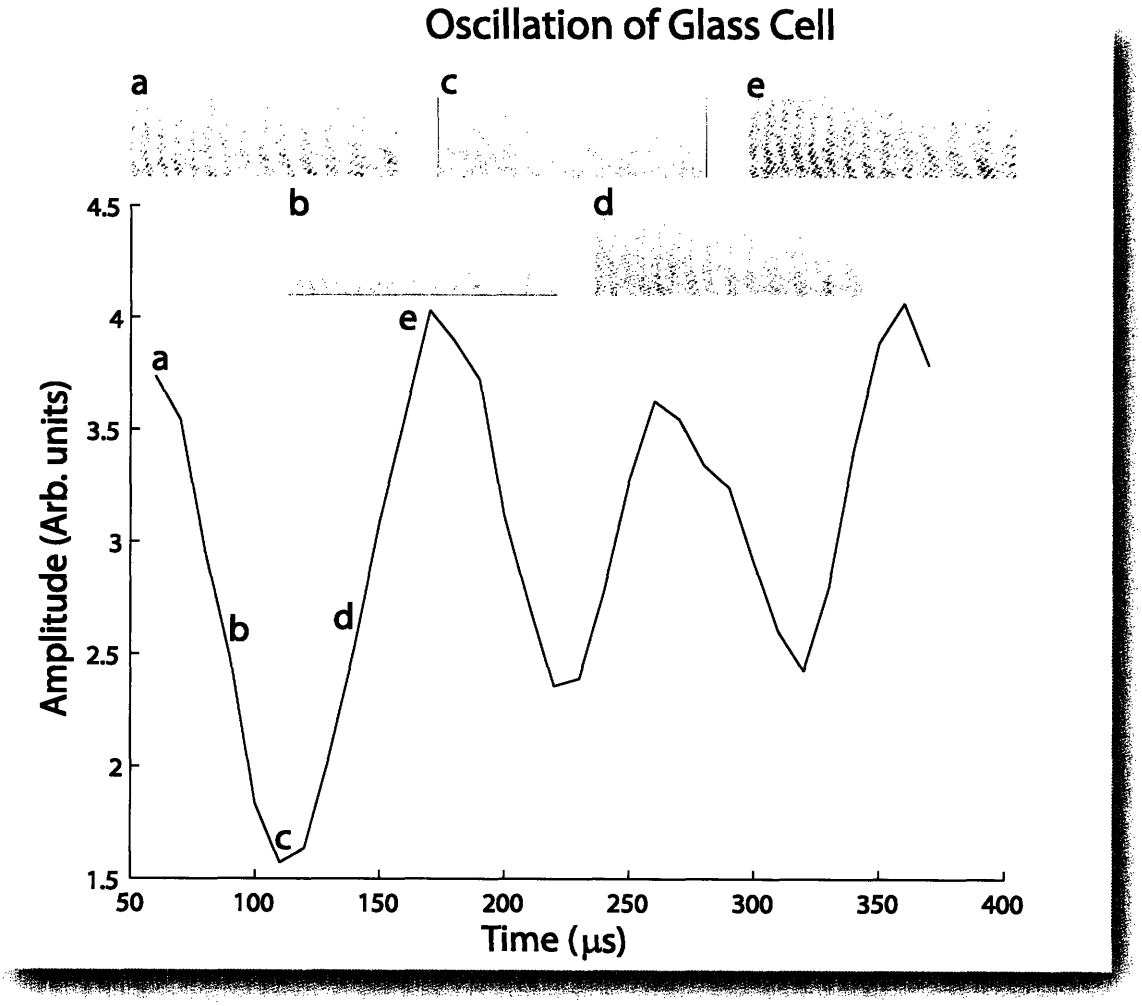

Figure 3-7. The vibration frequency data. The graph shows the amplitude of the interference fringes oscillates as we vary the time between the two images. Figure a to e shows some representative points in the graph.

Chapter 4

Experiment Control System

4.1 Hardware

BEC type experiments require precise timing of control signal to control the experiment. Currently we are using more than 60 digital channels, 12 analog channels, and 1 GPIB channel. Such complexity requires us to use a computer (or more) to control the experiment. Standard personal computers do not have the capabilities to give precisely timed digital and analog signal. Therefore, we use expansion cards from National Instruments to enable us to generate the digital, analog, and GPIB signal.

4.1.1 Digital Output Card

The digital output card consists of 32 channels capable of outputting digital signal at a maximum rate of 2 Mhz. The card communicates directly with the main computer memory using Direct Memory Access (DMA). In order to run an experiment, the computer must create a buffer for the output signal and store it in the main memory. The card has its own clock to output the buffer at user selected rate. For more accurate timing, the user can also provides an external clock to the card. Furthermore the card also allows us to phase lock the reference clock with other digital and analog cards in the system, making the relative timing drift between cards less than 1 μs.

4.1.2 Analog Output Card

The analog output card consists of 8 analog channels capable of outputting analog signal at a maximum rate of 500 Khz. The voltage resolution of the output is usually 12 or 16 bit. The card also takes the data directly from the main computer memory. As in the digital channel, the software has to create the output buffer and store it in the main computer memory. The analog card also has the same clock system as the digital output card.

4.1.3 GPIB Output

The GPIB card enables us to command any devices that can accept GPIB input. In our experiment, we use an Agilent signal generator for generating the RF and microwave signals that are used for evaporation. We use the GPIB card to command the signal generator what frequency and amplitude to

output with relatively precise timing. Different from the digital and analog cards, the GPIB card has neither internal clock nor the capabilities to accept external clock. Therefore, we must rely on the computer clock to time the GPIB command. This still allows us to have timing precision of about 15 ms, one thread cycle time of the computer. However, standard GPIB card is not suitable for applications where precise timing is required.

4.2 Old System (Word Generator)

The old system consists of 1 computer, 2 digital cards, 2 analog cards, and 1 GPIB card. The cards are housed in a single computer with 6 PCI slots. The software is home-made software written back in 2000. The software enables the user to create arbitrary signal for up to 1 minute. This system has enabled us to perform high quality physics experiments for the past 7 years. However, as the experiment becomes more complex, the system's limitation becomes more apparent.

4.3 Limitations of the Old System

4.3.1 Software Maintenance

Unfortunately, the software source code design does not follow acceptable software writing standard. The source code uses non-self explanatory variables, classes, and files names such as "face", "dna", and "mouth." The data structure is dominated by global variable style instead of object oriented style. There is no specification or documentation in both classes and methods. There were several people, including myself, who tried to modify and extend the software in the past without much success.

4.3.2 Timing Resolution

Although the theoretical precision of the cards are less than 1 μs, because of the limitation of the total PCI bandwidth, combined with multiple cards in a single computer, the cards cannot be run at the maximum clock speed. The old system only allows maximum precession of 10 μs. Although this was enough in the past, as the experiment grows, we need a more precise timing system. Currently we use a separate auxiliary system to generate fast signals. However this method unnecessarily increases the complexity of the system.

4.3.3 Scalability

The current size of the experiment makes the 64 digital channels and 24 analog channels limitation a burden. Although we solve this problem by multiplexing many of the digital channels using some logic circuits, we inadvertently increase the complexity of the system. In several occasions, we spent an entire day trying to locate a problem in the experiment, only to find out late in the day that we forgot that we already multiplexed a digital channel to control several equipments at the same time. This kind of problem can be eliminated with proper system design.

4.3.4 Physical Location

Our experiment is spread out throughout 3 optical tables and 6 electronic racks across two rooms. However, since there is only one control computer, the control system can only be physically placed in one location. This creates problems on routing the signal throughout the lab. We currently have BNC busses consisting of more than 80 long BNC cables with sole purpose to transfer signals from the control computer to other side of the lab. With that many BNC cables in the system, it is often the case that some of them are not properly connected, compromising the reliability of the experiment as a whole.

4.3.5 Lack of Automation Feature

The old software lacks one very essential feature: automation. The software allows the user to set up only one experiment at a time. This was acceptable in the past when the experiments were simple and did not require a huge amount of data. However, as the complexity of the experiment grows, each experiment requires more and more data, and manually inputting the running parameter becomes tedious and prone to human error. Automatic data taking with minimal human intervention becomes a necessity.

4.4 New System

The design of the new system solves all of the limitations mentioned above. This can be achieved by changing both the hardware and software design. At the time of writing, the new system is mostly completed. However, the new system is still not used in the experiment due to the lack of testing time.

4.5 New Hardware

4.5.1 Architecture

Instead of using a single computer, the new system uses multiple computers simultaneously, connected to each other via the Ethernet. The overall diagram is shown in Figure 4-1. This hardware design approach solves the timing, scalability, and physical location limitations of the previous design. The timing limitation was primarily caused by the PCI bandwidth of the computer. This can be solved by putting fewer cards in one computer so that the bandwidth is only shard by 2 or 3 cards. We can add more channels in the system simply by adding more computers without losing the output rate. Once a system of several computers is implemented, adding more computers would be a trivial task, solving the scalability issue. With multiple computers, it is also trivial thing to distribute the computers across the lab thus eliminating the excessive use of BNC busses in the lab.

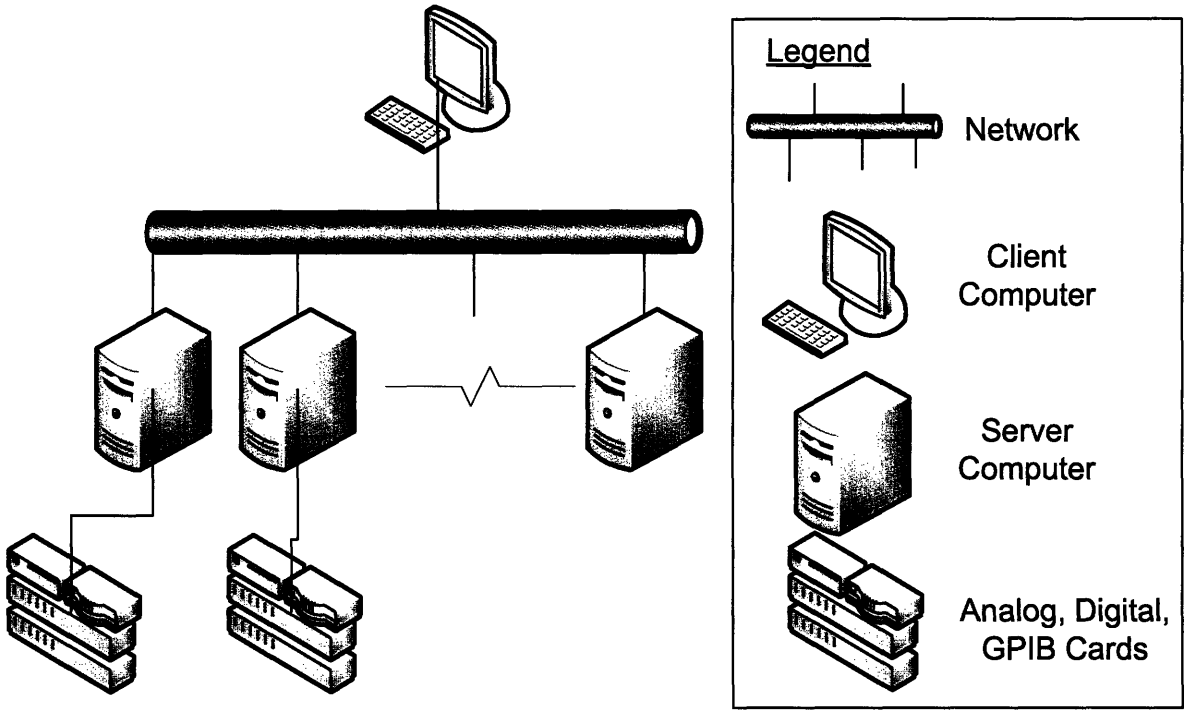

Figure 4-1. The overall view of the new system. There is a single client computer where we can program the system. The client computer is connected to several sever computers, each carrying analog, digital, and/or GPIB cards.

4.5.2 Possible Problems

Unfortunately, the multi computer approach also increases the complexity of the system considerably. In order the system to work, every single computer in the system must work flawlessly. Furthermore, they must be connected through Ethernet connection at all time. The new system might potentially increase the downtime of the experiment.

Synchronizing multiple computers with $0.1\mu s$ resolution will also increase the complexity of the system. The old single computer approach has the advantage that we can internally phase lock the internal clocks of all cards such that the drift between the cards is less than $0.1\mu s$. On the other hand, the new system must rely on clock and trigger signals to be routed across the lab.

4.6 New Software – X Generator

The new software, the X Generator, is written using Microsoft Visual Studio 2005 languages, which is also known as the .NET Framework. I will primarily use the C# language of the .NET framework. This language has the advantage of true build-in object oriented features, which makes the code more manageable, solving the maintainability problem of the old software. Furthermore, the .NET framework is so widespread that we can easily use many libraries that are freely available on the internet, reducing the development time.

The X Generator uses the standard client-server architecture. The system has a single client and several server instances running. Note that it is entirely possible to run the server program on the same computer as the client program as the distinction between client and server is only a logical distinction.

The X Generator also takes advantage of the recently available multi core processor by generating the output buffer in parallel, using all processor cores. This is important because increasing the timing resolution also means increasing the amount of output buffer that has to be generated.

4.7 X Generator – Client

The main control panel of the X Generator is shown in Figure 4-2. We see the overall experimental sequence in one page. The first section on the top shows the sequence control where user can select the timing of each step. The second section shows the analog signal where user can see how each analog channel changes at every step. The third section is the digital channel where user can change each digital channel state for each step.

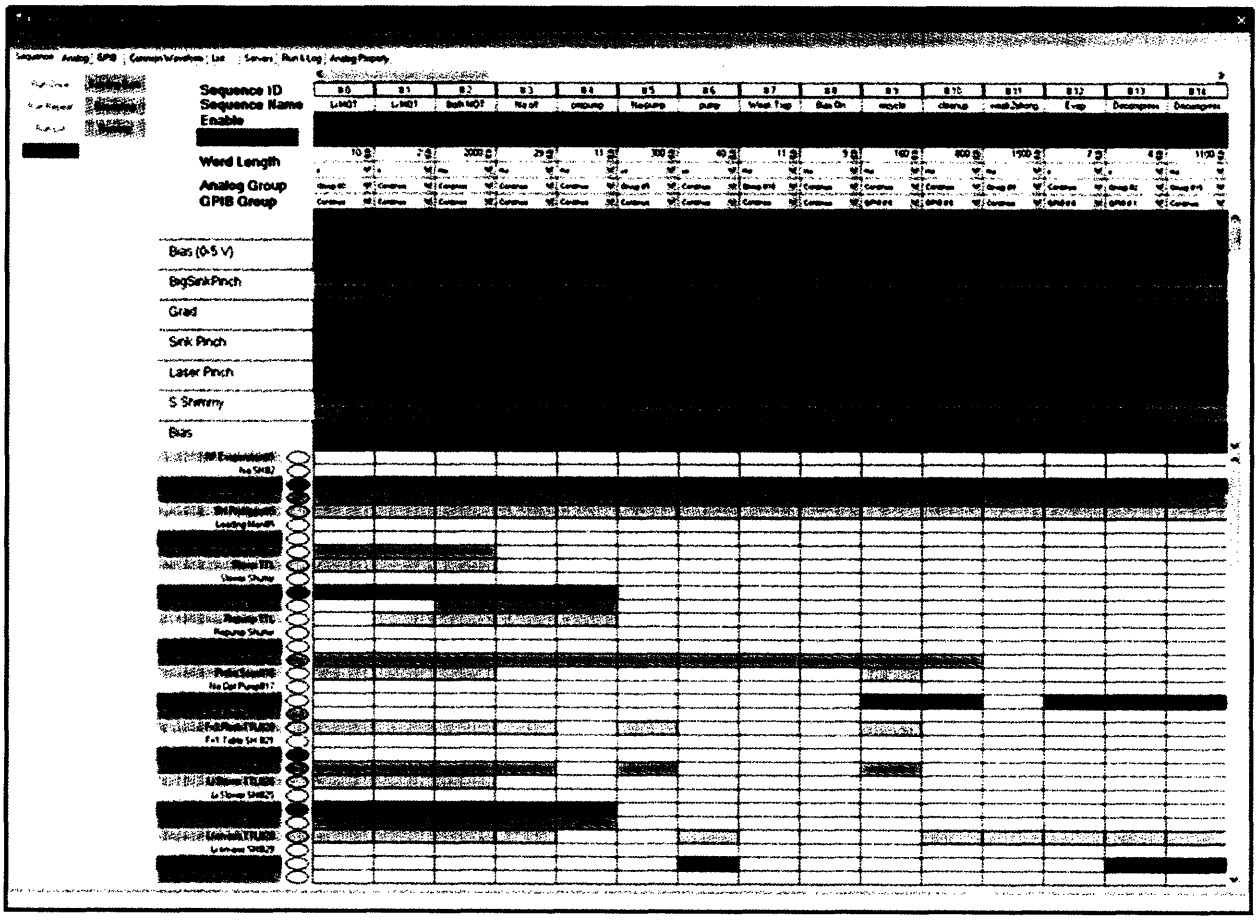

Figure 4-2. Main Control Panel of X Generator

4.7.1 Sequence Control

The primary framework of the software is the sequence control shown in Figure 4-3. The entire system revolves around the sequence control. The sequence control defines the important phases of the experiment. For example, creating a BEC involves about 30 phases such as MOT Loading, pumping, evaporation, time of flight, and imaging.

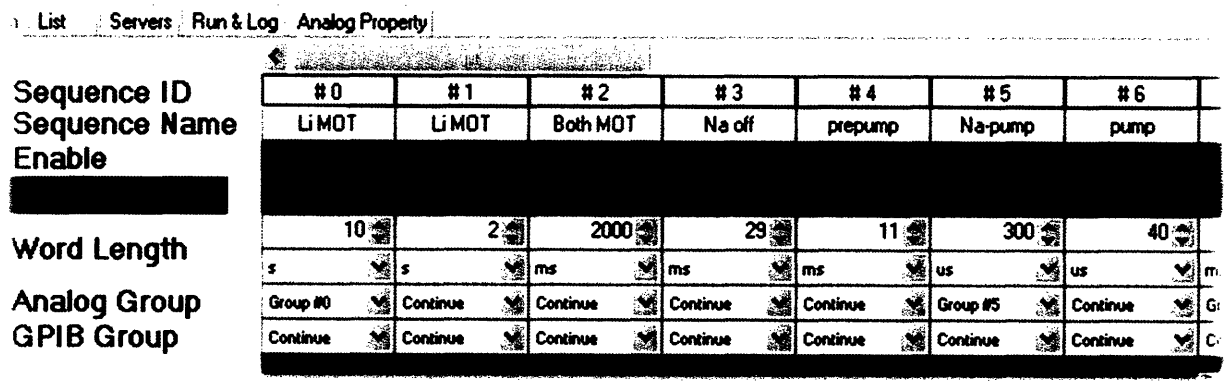

Figure 4-3. Close up view of the Sequence Control

The basic sequence control concept is taken from the Word Generator. The horizontal axis represents the time axis. The vertical axis represents hardware to be controlled for particular time such as the digital channels, analog channels, and GPIB channels.

One new feature in the new sequence control is the variable time feature. Instead of specifying the time of each phase in absolute quantity, user can select a variable for that phase. The software then will make the length of the phase to be the value of the variable. This is useful in at least 2 scenarios:

1. Changing a parameter that drifts form day to day. One good example is the optical pumping time. In order to create a stretched state in the magnetic trap, we have to pump the atoms with optical pumping light for an exact duration. Unfortunately, for some reason the optimum duration changes from day to day. What we can do is to put the length of this phase to be a variable, and specify the value of the variable once for the entire day. This way, we do not have to readjust the pumping time whenever we open a new program. This feature will reduce the typical human error of forgetting to change the value of a parameter whenever opening a new program.
2. Scanning the length of one phase. The idea is to take the value of the variable based on the value of a list (see Section 4.7.5).This is useful when we are taking data for a measurement. For example, we can scan the trap holding time to figure out the decay time constant of the atoms.

4.7.2 Digital Control

The basic control of the digital panel is taken from the old software. The panel consists of a 2D grid of buttons. The horizontal axis represents the time axis while the vertical axis represents different digital channels. Each button has 2 states, ON and OFF. This enables the user to output an arbitrary sequence of digital signals on every channel.

One new feature of the digital panel is the automation feature. Rather than specifying ON or OFF state for each button, user can simply right click on the button to enable the variable method. The value of the button now depends on the value of the chosen variable. This feature is useful for 2 things:

1. User can make many buttons to refer to a single variable. This way, by simply changing the value of one variable, the user can change the value of multiple buttons simultaneously. This is useful for example when we want to choose to use side imaging or top imaging. Changing the imaging axis involves changing multiple digital signals at multiple channels simultaneously which is simplified greatly by this feature.
2. User can use the automation feature for the particular button. The idea is to take the value of the variable based on a list of possible values. See Automation Feature section below.

4.7.3 Analog Control

The concept of analog control is a little bit different from the concept of digital control. Rather than specifying the value of each analog channel at every phase, we specify the analog group. An analog group is a set of possible changes for each analog channel at every single phase of the experiment. See Figure 4-3 in the analog group section. If there is no change in the analog values, user can simply set the analog group to "continue." If there is a change for an analog channel in that group, the user can specify a new waveform to represent the change by choosing a new analog group.

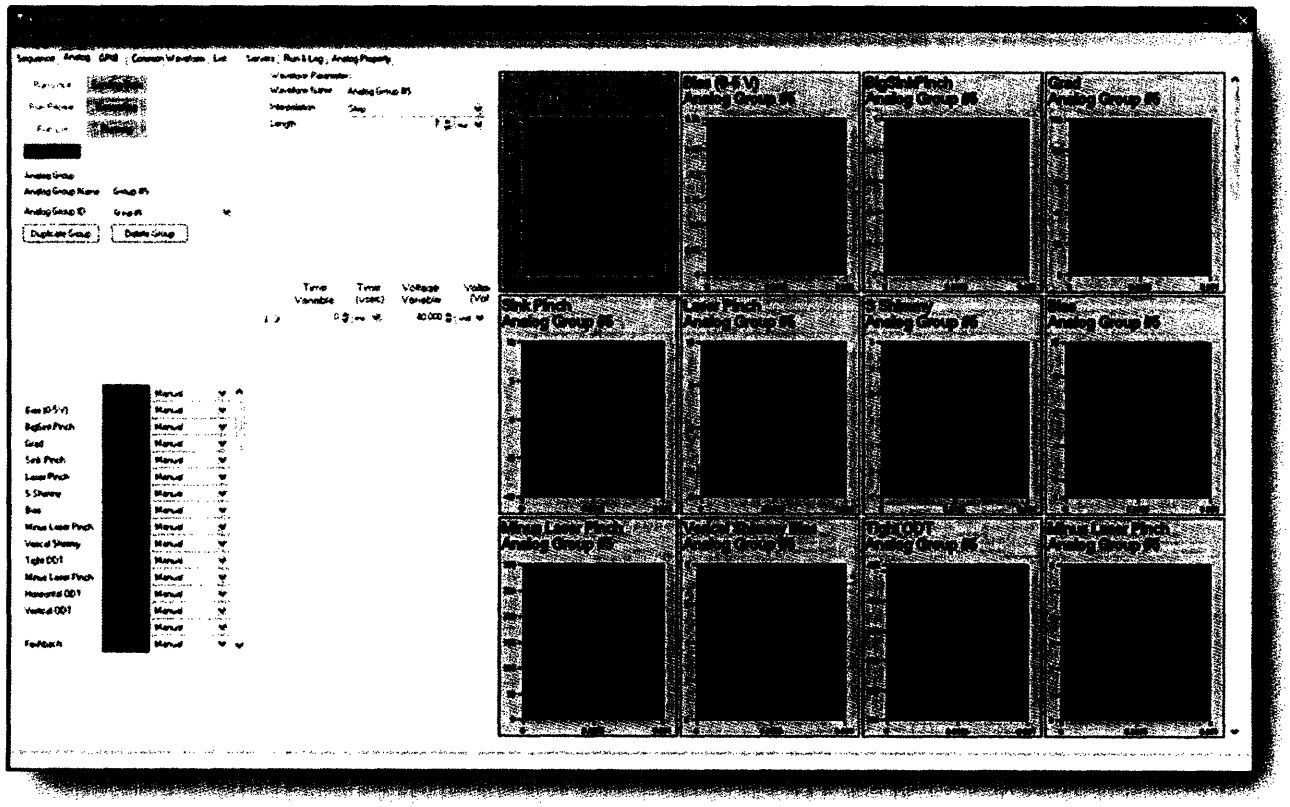

Figure 4-4. AnalogWaveform Control

Analog Waveform

An analog waveform is a sequence of voltages as a function of time. The user interface is shown in Figure 4-4. Each graph in the figure represents an analog waveform. Usually an analog waveform represents the voltage of a single analog channel for one phase of the experiment. However, depending on the application, a single waveform can also span more than one experimental phase.

There are 2 kinds of waveform:

1. Standard Waveform
   Standard waveform is specified by defining a voltage at each key time point. There are many interpolations and approximations possible for a standard waveform such as linear interpolation, step interpolation, cubic spline interpolation, and bezzier approximation.
2. Special Waveform
   Special waveform is specified by giving several key parameters for that waveform. Some possible special waveforms are exponential, sinusoidal, and basic spline ramp. For example, user can define a sinusoidal waveform by giving the frequency, phase, amplitude, and offset.

Common Waveforms

Common waveforms are a collection of analog waveform that is not tied to any specific analog channel. One application of common waveform is when creating a 3D lattice. To create a 3D lattice, user has to specify the amplitude of the laser beam for all 3 possible axes. Usually, the shapes of all three lattice beams are the same. The only difference is the scaling between different axes. Instead of specifying an independent waveform for each lattice beam, user can create a single common waveform for all three beams. The user can then specify the scaling for each beam.

Variable and Automation Feature

Similar with the sequence control and the digital control, all time and voltages values in each waveform can be set to a variable value. User can then dynamically change the shape of the waveform by reading the value of each variable from the pre-defined list.

4.7.4 GPIB Control

The GPIB control concept is also taken from the Word Generator. Same with analog channel, at each phase of the experiment, we choose a group for the GPIB channels.

4.7.5 Automation Feature

The new software has an automation feature build in as shown in Figure 4-5. User can simply input a variable instead of an absolute value for every possible output in the program. The program in turn will in turn substitute the variable with a value chosen from a list of values. For example, instead of specifying that the voltage at t = 0 should be 5 Volt, the user can specify it to be x Volt. The user then input a list, where the program will substitute x with one of the values in the list.

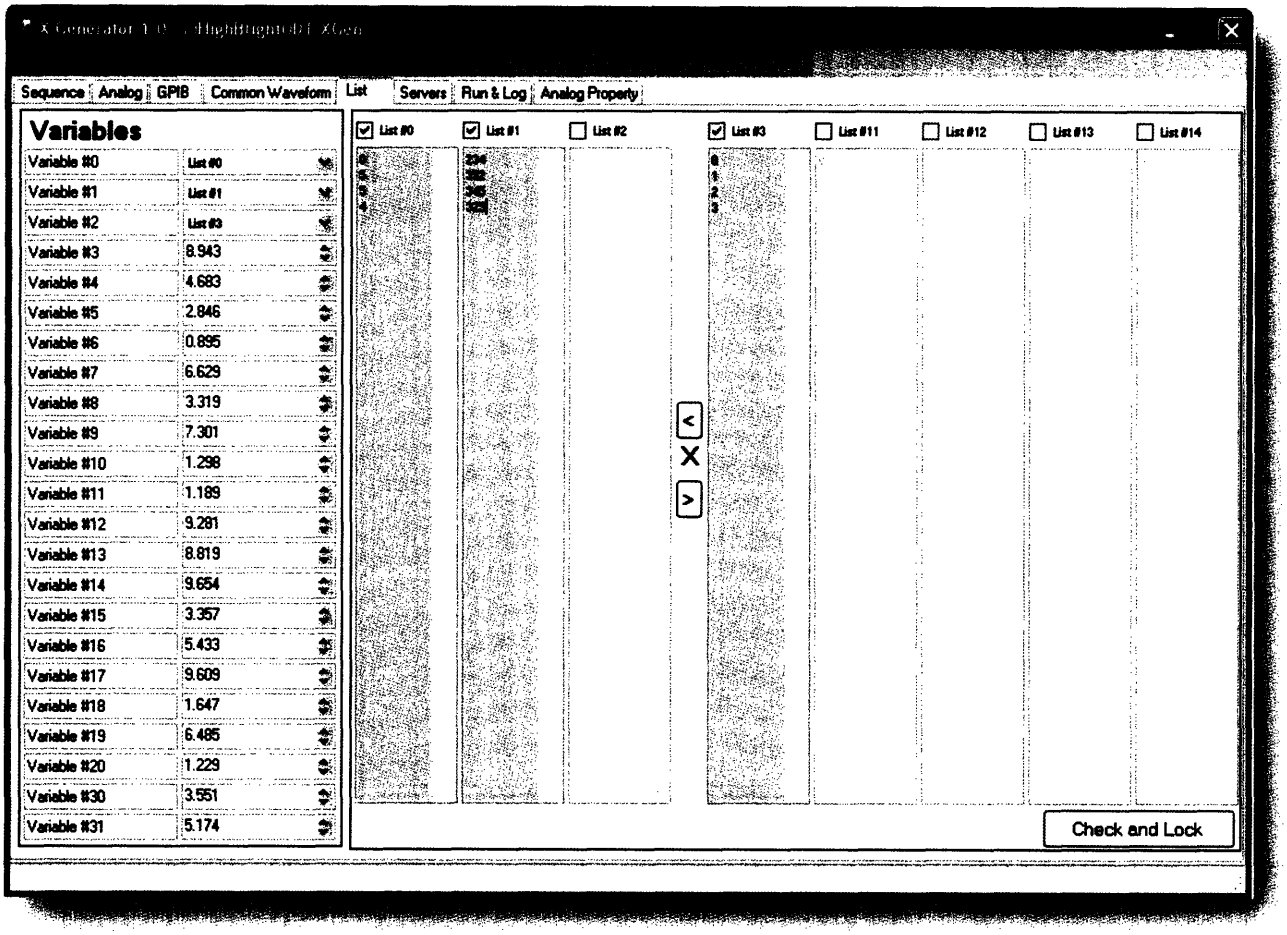

Figure 4-5. Automation. User can input a list of values that will be generated for each experiment.

The automation feature will minimize human intervention when taking a large set of data, reducing the possibility of human error.

4.7.6 Serial Control

One feature that has not been integrated in the new software is a serial control feature. However, this feature is implemented in the auxiliary control program that is called the X Scanner (see Appendix C). The serial control is capable of giving commands to a device that can accept the serial port for example the IPG YAG laser, SRS controller, and the Agilent function generator. This feature is one of many key components which enable us to take many data points for any given measurement such as in the critical velocity experiment.

4.8 X Generator – Server

The other component of the X Generator is the server, shown in Figure 4-6. Each server instance controls all hardware on a single computer. There can be multiple servers that can be controlled by the

client software simultaneously. The client software sends the correct command for each server automatically, making the existence of the server transparent from the user. The user can control the experiment as if there is only one computer in the entire experiment.

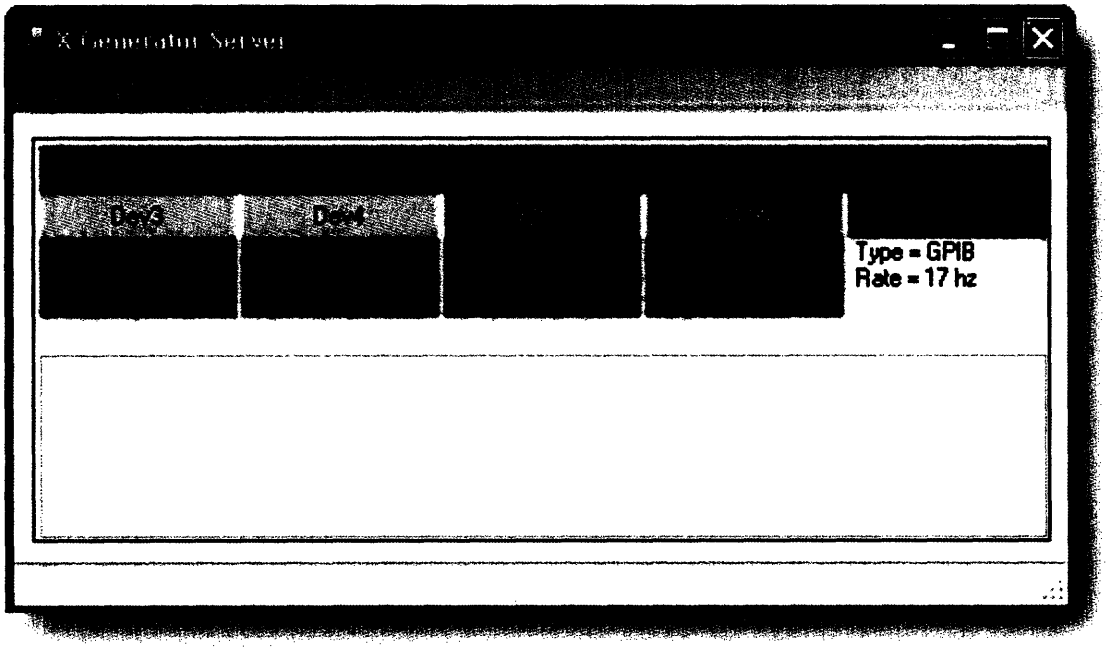

Figure 4-6. X Generator Server

4.9 X Generator – Legacy Parser

The process of upgrading to new software is not finished by simply writing the new software. We still have to take the data from the old software and incorporate it to the new software. To facilitate the upgrading process, software called the Legacy Parser can transform the old data format into the new data format. This software will make the upgrading process seamless.

4.10 Conclusion

With more than 15,000 lines of code, the X Generator project is by far the most complex project I have ever done. As a comparison, this thesis only consists of about 1,200 lines. At the time of writing, we are still in the process of upgrading to the new software. This software should be able to increase the productivity of the lab in the near future.

Chapter 5

Conclusion

My journey as a physicist started when I joined Wolfgang Ketterle's lab. I joined with neither technical nor experimental skill. Soon after I joined, the lab decided to pursue a new research direction in degenerate fermionic gases. Over the following two years I developed an appreciation for the big picture of experimental physics, from designing the new system and ordering equipment to getting first results and publishing scientific papers.

My first project was to build an AOM driver, followed by an IGBT driver, and a PID controller. Over the course of 3 years, I ended up making at least 25 channels of AOM driver, 4 IGBT drivers, and 20 channels of PID controllers. Some of them are still in use, while many are already replaced with better versions.

In the second year, I started to learn software programming techniques. At the time, the primary motivation was to fill in the knowledge gap in the lab, since no other lab member knows enough about programming. MIT is certainly one of the best places to learn software engineering skills. I immediately applied the knowledge that I learned to create new software or rewrite old software in the lab. As my skill improved, the project became more complicated, with the X Generator as the most complex project.

I also learned some optics skills, although relatively slowly. The reason was because most of the optics projects were taken by the graduate students and post doc. However, in the end, I was able to setup a new laser system for the lithium atoms during the winter break when most people were not in the lab.

The process of upgrading the machine was full of setbacks, such as Argon laser problem, leaks in the vacuum chamber, unstable diode laser, and noisy imaging system. However, we solved those problems one at a time, and we are at the stage to be able to produce scientific results. I expect many good results from this lab in the near future. It is unfortunate for me to leave the lab just when the upgrade process is completed.

I have been working in this lab for three years which is relatively long for an undergraduate. I started with neither experience nor knowledge in technical things and ended up with many skills required for experimental physics. This knowledge will certainly help me in my future career as a physicist.

Appendix

A Microcontroller Based Analog Device (X Analog)

A.1 Introduction

Before we use the TOPTICA laser system for our lithium setup, we tried to create our own laser diode system. One critical component in any laser diode system is the temperature controller. Unfortunately, our optical table is filled with noise from other equipments such as fans, electronics, RF amplifier, and AOM. This noise made pure analog temperature controller unstable. The final stabilized temperature still oscillates in tens of milli Kelvin, although I must admit that the analog temperature controller was not designed with precision in mind.

One method that works well for temperature stabilization is a micro controller based PID controller. Even the simplest modern microcontroller runs at 60 Mhz, which is much faster than typical temperature oscillation time scale. The microcontroller is also equipped with 512 KB of flash memory and 32 KB of RAM, making it a very versatile device. Using microcontroller, it is possible to produce several outputs based on arbitrary computations of several inputs, limited only by the processing speed. The idea is to use this computing power to create a sophisticated temperature control system, filtering all noise in the system.

Unfortunately, soon after I started to develop this microcontroller based PID controller, the diode laser system was abandoned in favor of the dye laser setup. However, I still continued the project partly because of personal curiosity and partly because I expect that this device should be universal enough to be used in many different applications in the future. Here I present the basic design of this analog device.

A.2 Hardware

For the microcontroller, I use the Philips LPC2148 ARM microcontroller. The microcontroller is chosen because it is the latest generation of microcontroller with very strong user base. The microcontroller is equipped with 60 Mhz processor, USB port, 2 serial ports, two 10-bit ADC, 8-bit DAC, and 48 digital ports. The price tag of this device is less than $10 which is negligible.

One down side about modern microcontrollers is the physical size, which is almost microscopic. This particular ARM microcontroller is only 1 cm x 1 cm but it has 64 pins (that is 16 pins/cm). To ease the soldering task, I decided to use a prototype board instead using the chip directly. I use LPC2148 USB QuickStart Board from Embedded Artist shown in Figure A - 1. The board also provides a crystal oscillator while increasing the overall board size such that the pin density is only about 4 pins/cm. This makes the soldering task much easier.

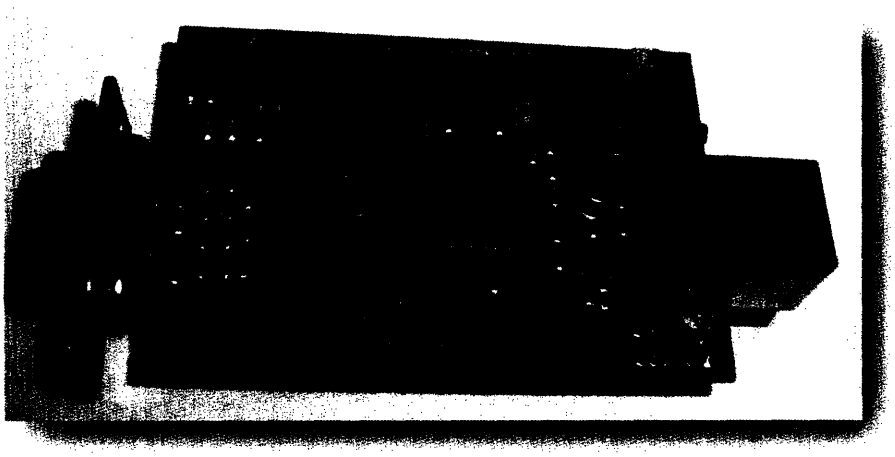

Figure A - 1. Embedded Artist LPC2148 USB QuickStart Board.

One of the primary goals of this project is to make the feedback system as flexible as possible so that the feedback system can be reused for other tasks. Therefore, the feedback system supports 3 ADC and 3 DAC simultaneously. To improve precision, both the DAC and ADC have 16 bit accuracy with 100 khz sampling rate. The sizes of the component are chosen to be as small as possible to reduce the overall size of the device. Therefore, all of the components in the feedback system are surface mount components mounted on a double layer PCB.

A.3 Electrical Connection

The electrical connection of the PCB board is shown in Figure A - 2. The quick start board is connected to 3 DAC and 3 ADC using the 16 bit bus. There are several other control lines connected to each DAC and ADC that are not shown in the diagram. The X Analog can also communicate with another device (such as a computer) via the serial port. The complete schematic is shown in Figure A - 3. The component layout of the PCB board is shown in Figure A - 4, and the assembled X Analog is shown in Figure A - 5.

Figure A - 2. Simplified schematic of the X Analog

The components for the feedback module are:

a. Embedded Artist LPC 2148 Quick Start board
   LPC 2148 equipped with serial connector, oscillator, and header for all pins in the LPC2148 microcontroller. This board is chosen because the size of the microcontroller is very small which makes it very hard to solder. The board also has a 5 volt to 3.3 volt converter. This feature is useful because most equipment uses 5 volt power supply. The board also has a USB connector so that we can power the board from a USB port. On design part, this board makes the system more modular because we can just replace the board if we want to change the software in the implemented system. The PCB board is designed such that we can mount the quick start board directly to the PCB board without any soldering.
b. DAC712U, DAC
   16 bit, 100 khz DAC module. 28-SOIC connection
c. ADS7805, ADC
   16 bit, 100 khz, ADC module, 28-SOIC connection
d. T491B106K020AS, bypass capacitor
   10 uF tantalum capacitor, 3528 SMD connection

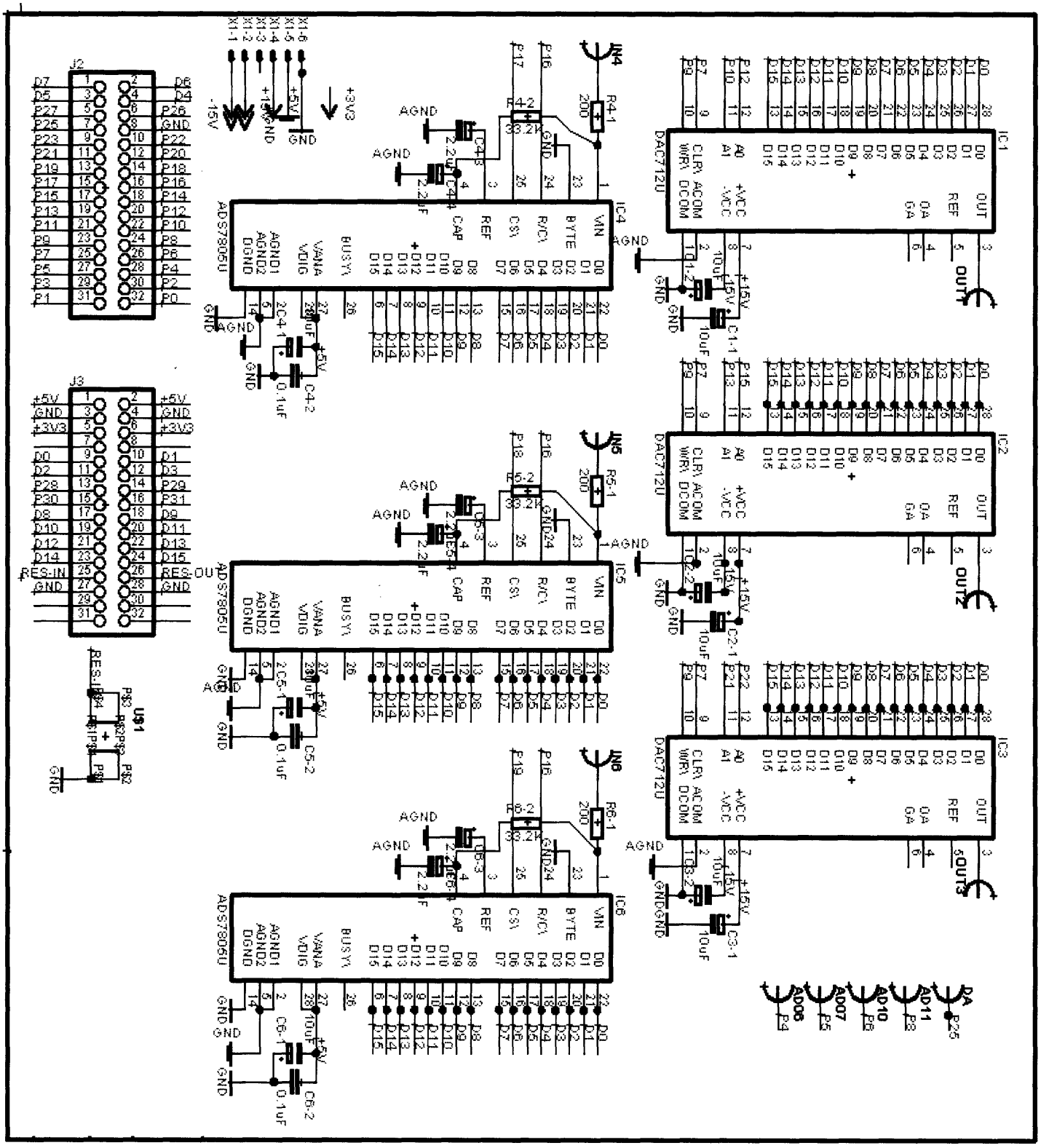

Figure A - 3. The complete schematic of the X Analog.

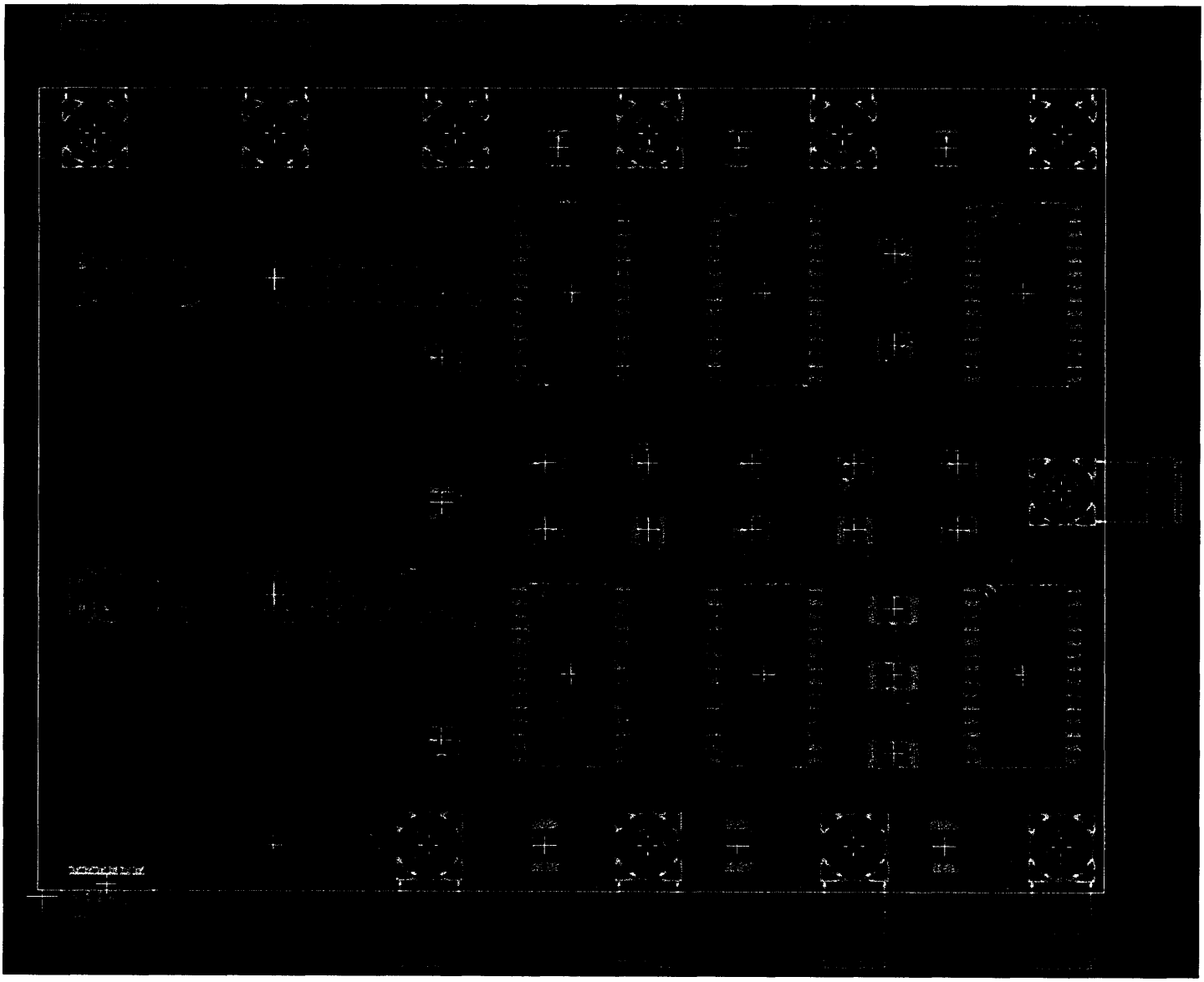

Figure A - 4. The component layout of the PCB board.

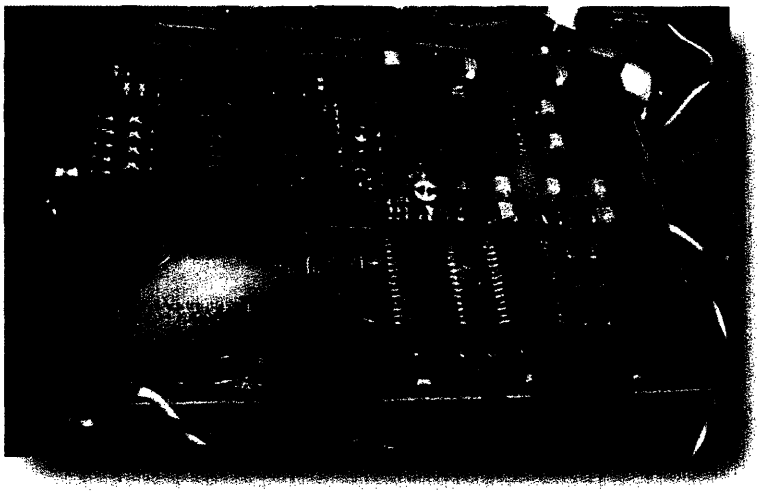

Figure A - 5. The complete X Analog.

The LPC 2148 microcontroller itself has 48 General Purpose Input Output (GPIO) which are divided into port 0 (32 GPIO) and port 1 (16 GPIO). The entire port 1 is used as the data bus. Port 0 is used to control each DAC and ADC independently without any demultiplexer. The direct control makes it possible to address multiple chips simultaneously. This is useful for example when we want to output the same data to several DAC, or to pass data from ADC to DAC directly without using the microcontroller. The Port 0 Configuration is:

Port 0 configuration

Pin	Function
0	UART0-TXD
1	UART0-RXD
2	Noisy
3	Noisy
4	Internal AD0.6
5	Internal AD0.7
6	Internal AD1.0
7	DAC-CLR
8	Internal AD1.1
9	DAC-WR
10	DAC1-A1
11	Noisy
12	DAC1-A0
13	DAC2-A1
14	Noisy
15	DAC2-A0

Pin	Function
16	ADC-RC
17	ADC4-CS
18	ADC5-CS
19	ADC6-CS
20	ADC7-CS
21	DAC3-A1
22	DAC3-A0
23	Reserved
24	Reserved
25	DAC
26	USB-Out
27	USB-In
28	DAC0-A1
29	DAC0-A0
30	Unused
31	Out only

For basic PID setup, we can use ADC 1 as the input, DAC 1 as the output, leaving the other 4 ports unconnected.

A.4 Software

The software of the X Analog is written in C++ making it possible to write a fairly complex program. However, for demonstration purpose, I only wrote a simple PID program. The basic setup of the program in shown in Figure A - 6

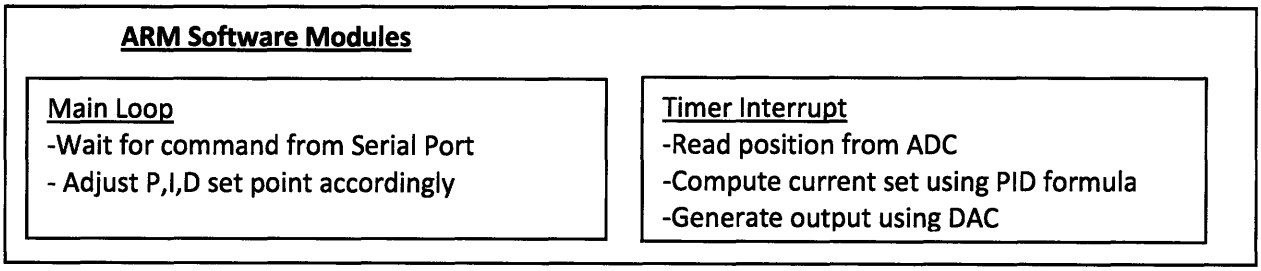

Figure A - 6. The software architecture of the X Analog

The software located on the ARM microcontroller can be divided into two almost independent parts: the Main Loop thread and the Timer Interrupt thread as shown in Figure 8 above. The Main Loop waits for command from the serial port and adjusts the PID settings and Set Point accordingly. The Timer Interrupt part periodically reads position data from the ADC, computes the appropriate output using the PID formula, and generates the output using the DAC.

A.4.1 Serial Port Communication Protocol of the X Analog

For serial communication purpose, the X Analog is configured as a passive device: the analog device never starts any serial communication with other device. The communication is always initiated by the outside device. The communication is done through the serial port with following parameters:

- 8 bits
- No parity bit
- 1 Stop bit
- 9600 Baud Rate

The communication is done using question-answer pattern: outside device asks a question to the X Analog, and the X Analog returns an answer. Both question and answer are always started by 0x31 0x41 and ended by 0x0D 0x0A.

Let us define a data type **short**. **short** is a 2-**byte** integer that can be represented as:

short = High Byte : Low Byte

The format of the question is:

0x31 0x41 questionCode byte1 byte2 .... byteN 0x0D 0x0A

where questionCode is a **byte** with the following possible values:

Code	Name	Description	Number of

			Parameters
0x00	Ping	Ask the UPID to return an answer. The returned answer is "pong"	0
0x01	Set P	Set the Proportionality constant on the UPID Parameters: (**short** value) New P = Value / 1000	2
0x02	Set I	Set the Integration constant on the UPID Parameters: (**short** value) New I = Value / 10000	2
0x03	Set D	Set the Differentiator constant on the UPID Parameters: (**short** value) New D = Value / 100	2
0x04	Set setPoint	Set the Set Point of the UPID Parameters: (**short** value) New setPoint = Value (in mV)	2

A.5 Computer Software

The final step to use the X Analog is to write software in the computer side. The software communicates with the X Analog via the serial port. Currently the software is capable of adjusting the PID setting and the set point of the X Analog PID controller. The snapshot of the software is shown in Figure A - 7.

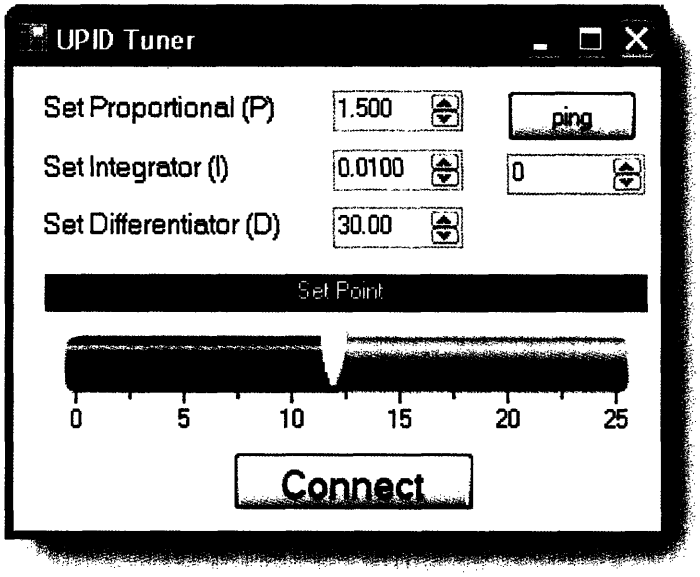

Figure A - 7. Snapshot of the software in the computer side.

A.6 Demonstration – Magnetic Levitation

To demonstrate the X Analog PID Controller, I created a magnetic levitation device. The setup is shown in Figure A - 8.

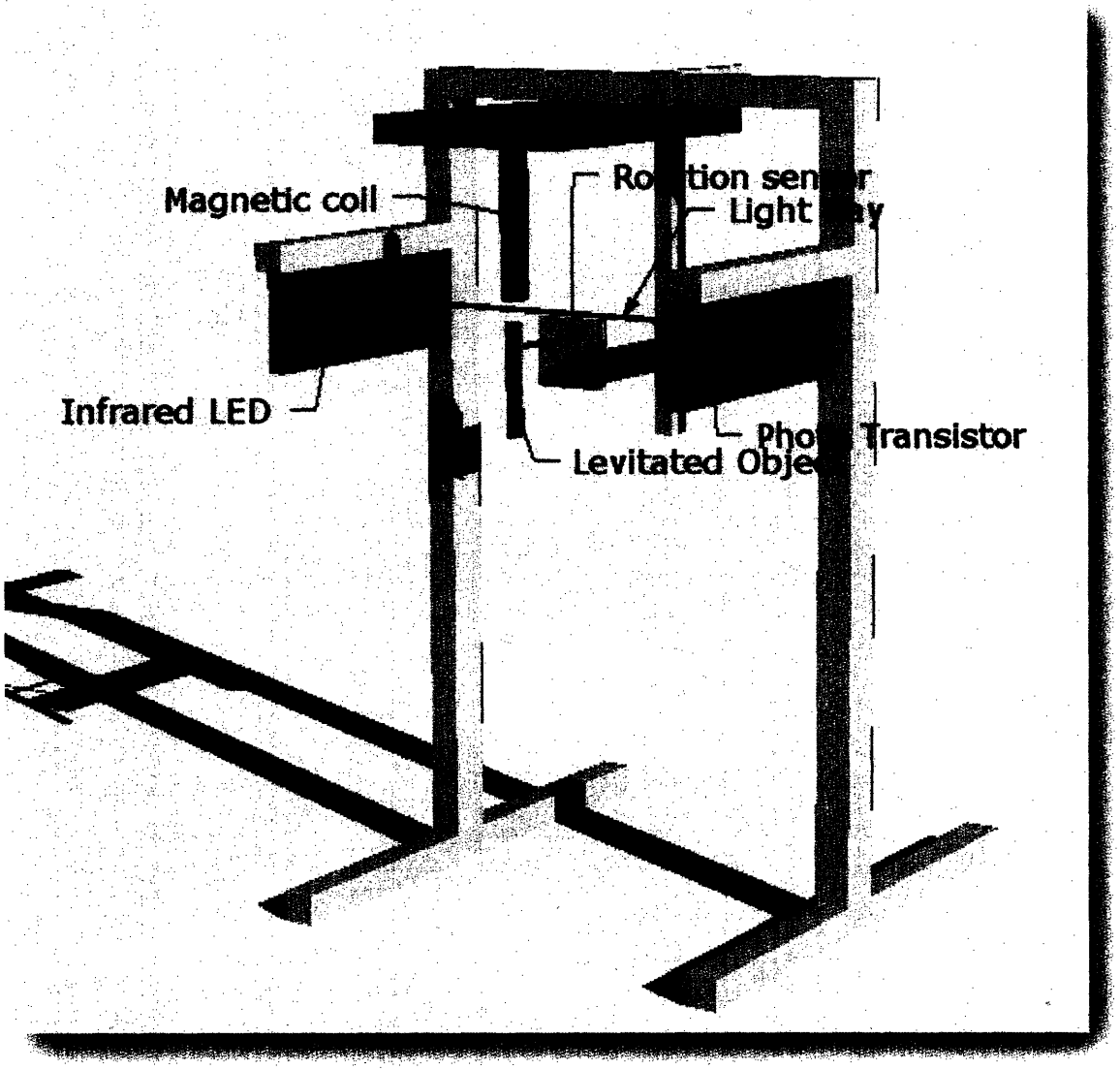

Figure A - 8. Magnetic Levitation Hardware

The hardware consists of 2 parts:

1. Magnetic coil: produces the magnetic field to pull the object
   The magnetic coil is made using a 3/8" steel core bolt and AWG 24 magnetic wire wrapped around approximately 1000 times. The magnetic coil is powered by a 12 Volt 2 amp power supply. The current is directly modulated by a 2N3055 power transistor. The current is then controlled using a feedback system using an op amp.
2. Infra red LED and photo transistor system
   Measures the location of the levitated object by measuring the amount of light that is not blocked by the levitated object.
   The infrared LED is OP 133 and the photo transistor is OP505A. The LED is always on. There are 2 photo transistors, one is directly in the line of sight of the LED, and the other one is located 2 cm

away. The signal is then the difference of the two phototransistors input. This method is used to subtract the background light level in the room.

The X Analog PID Controller successfully levitates objects using the feedback system. Note that both the P and D components are required for successful levitation. On average, the object can stay levitated for about a day before the object finally sticks to the coil or falls to the ground.

A.7 Conclusion

The X Analog PID Controller works as expected as demonstrated in the magnetic levitation device. However, it has not been tested for the intended temperature stabilization function.

B Multiscope

B.1 Introduction

As the experiment grows larger, there are more signals that have to be monitored constantly in order to make sure that everything works as it should. The traditional way of monitoring these signals is by using voltmeter or oscilloscope. However, monitoring many voltmeters and oscilloscopes simultaneously become more and more tedious as the number of signals to be monitored grows. One way to solve this problem is by automating the entire monitoring task. The easiest and the most flexible way of automatically monitor these signals is by using a computerized voltmeter/oscilloscope.

This project is designed to solve the monitoring problem above. The idea is to create a computer based oscilloscope with many channels and automatically compare the readout value with the predetermined parameters.

B.2 Hardware

We use the NI PCI-6220 card from National Instruments. The card is capable of reading 16 analog inputs at 16-Bit resolution with combined readout bandwidth of 250 kilo sample/second. The card is also equipped with 24 static digital input-output. The card itself is relatively cheap, around $400, or around $25/channel, comparable to a decent voltmeter, and much cheaper than an oscilloscope.

One major drawback of this card is the readout speed of about 15 kilo sample/second/channel. However, most of the signal that we monitored falls well below that range. For signal that need faster readout, we still rely on standard oscilloscopes.

B.3 Software

As usual, the software is written in C# language from Microsoft Visual Studio 2005. National Instruments provides a very organized device driver in this platform, making software development relatively simple.

The software mentioned below is prototype software with only the most basic functionality. A snapshot of the program is shown in Figure B - 1. The left side shows 9 of the 16 channels in oscilloscope style display. The right side displays the last readout voltage of all 16 channels in voltmeter style display.

In the oscilloscope display, for each channel, the user can select a trigger source (another channel). As in standard oscilloscope, the user can select the time scale of the signal from 1 ms to 10 seconds. Note that each oscilloscope display is independent of each other. It is possible to display the same channel triggered by different sources on two separate oscilloscopes.

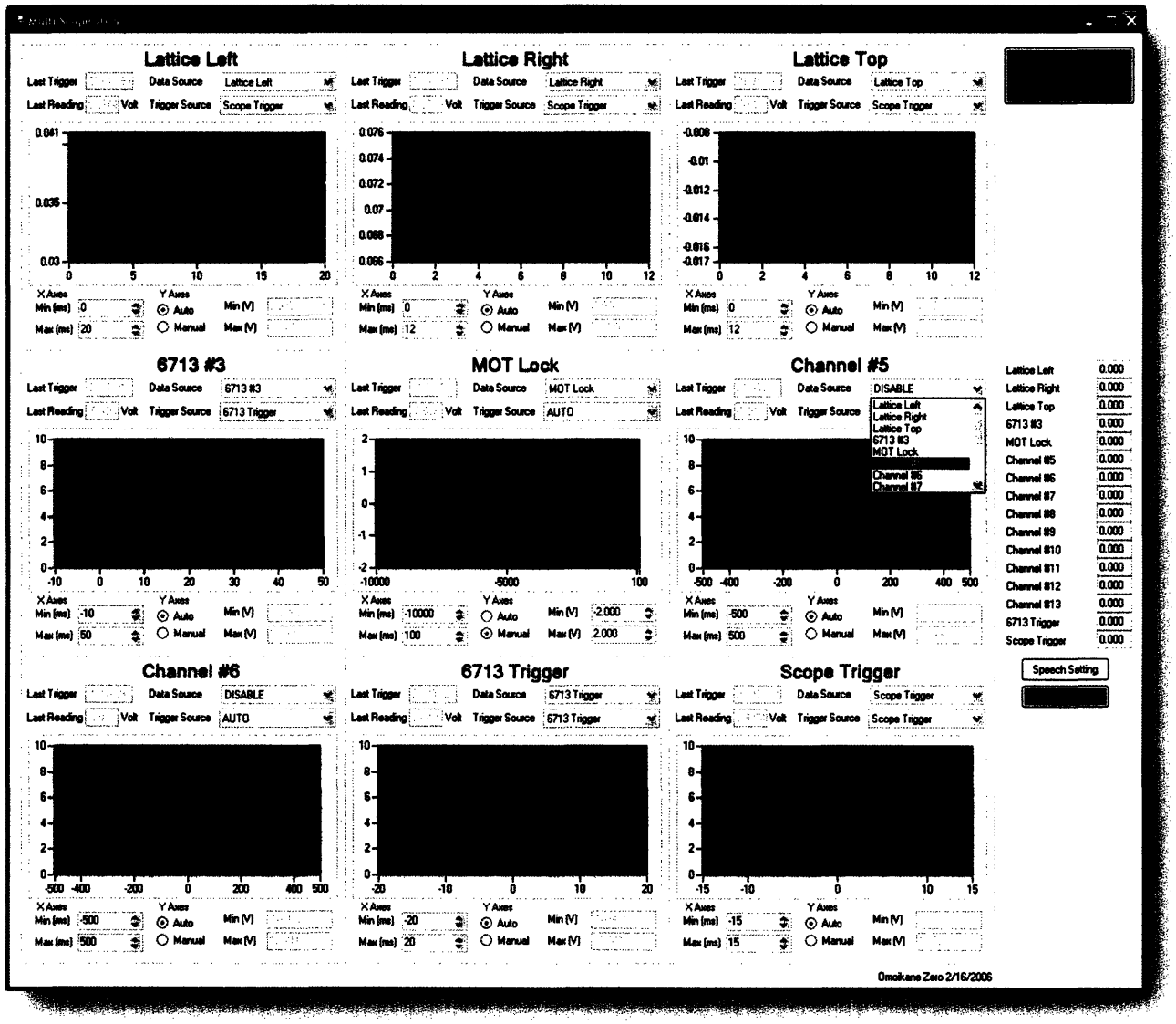

Figure B - 1. Snapshot of the Multiscope program.

The software is also equipped with a basic speech synthesizer. The snapshot is shown in Figure B - 2. User can define several ranges of values that can trigger the alarm and the description of this alarm. The software then will synthesize the alarm in human voice and say it out loud.

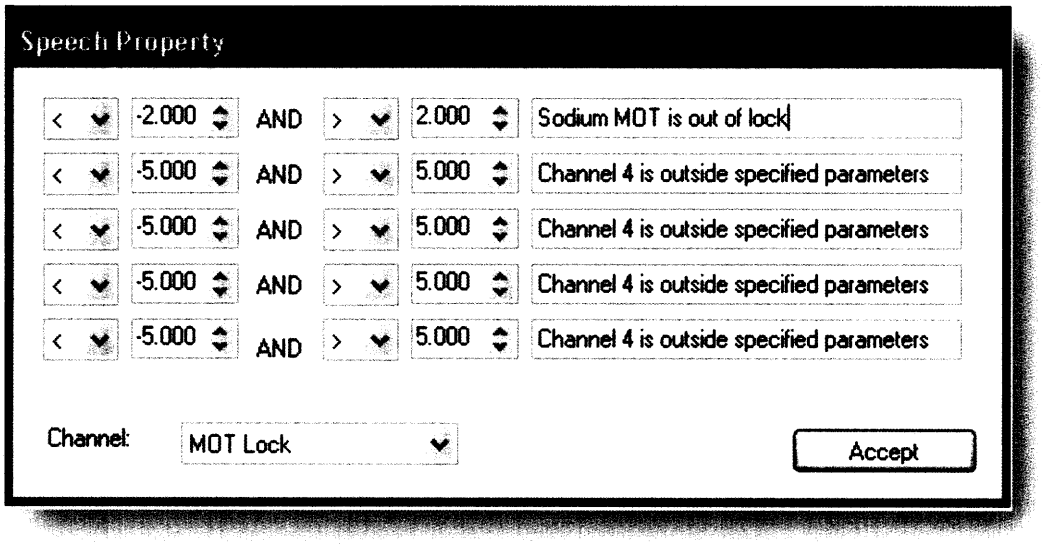

Figure B - 2. Snap shot of the speech enabled monitoring control.

One example of the application of this audible alarm is to monitor the laser lock. From time to time, the dye laser become out of lock (every few hours). The signature is when the driving voltage of the dye laser lock control is higher than 2 volt or lower than -2 volt. The program will then say "Sodium MOT is out of lock" several times, telling the user to re-lock the laser.

C X Scanner

C.1 Introduction

The scanner program is the prototype of the X Generator and thus written much earlier than the X Generator.

The old Word Generator program allows the user to control 64 digital channels, 16 analog channels, and 1 GPIB channel. The resolution of the digital and analog channel is 10 μs. For optical lattice application, this timing resolution is enough. There was auxiliary software called Scanner that can output analog signals at 1 μs resolution. However, even the combination of the old Word Generator and the Scanner still lack automation. At the time, I did not have any experience with the National Instruments cards. Therefore, rather than rewriting the entire Word Generator program, I decided to rewrite the much simpler scanner program instead, and I named the new program X Scanner.

The X Scanner program is originally designed to provide the user with automation feature especially for optical lattice applications. However, the program has grown to include serial control of the Agilent signal generator. In the end, this serial control automation feature became the critical feature for several experiments that required large amount of data such as the RF spectroscopy experiment and the critical velocity experiment.

C.2 Hardware

The Analog Output hardware is a PCI-6713 Analog Output card from National Instruments which was used by the old Scanner program. The function generator is the Agilent 33250A Function/Arbitrary Waveform Generator. The serial port is the build-in serial port in the computer.

C.3 Software

As you might expect, the software is written in C# from Microsoft Visual Studio 2005 using .NET Framework 2.0.

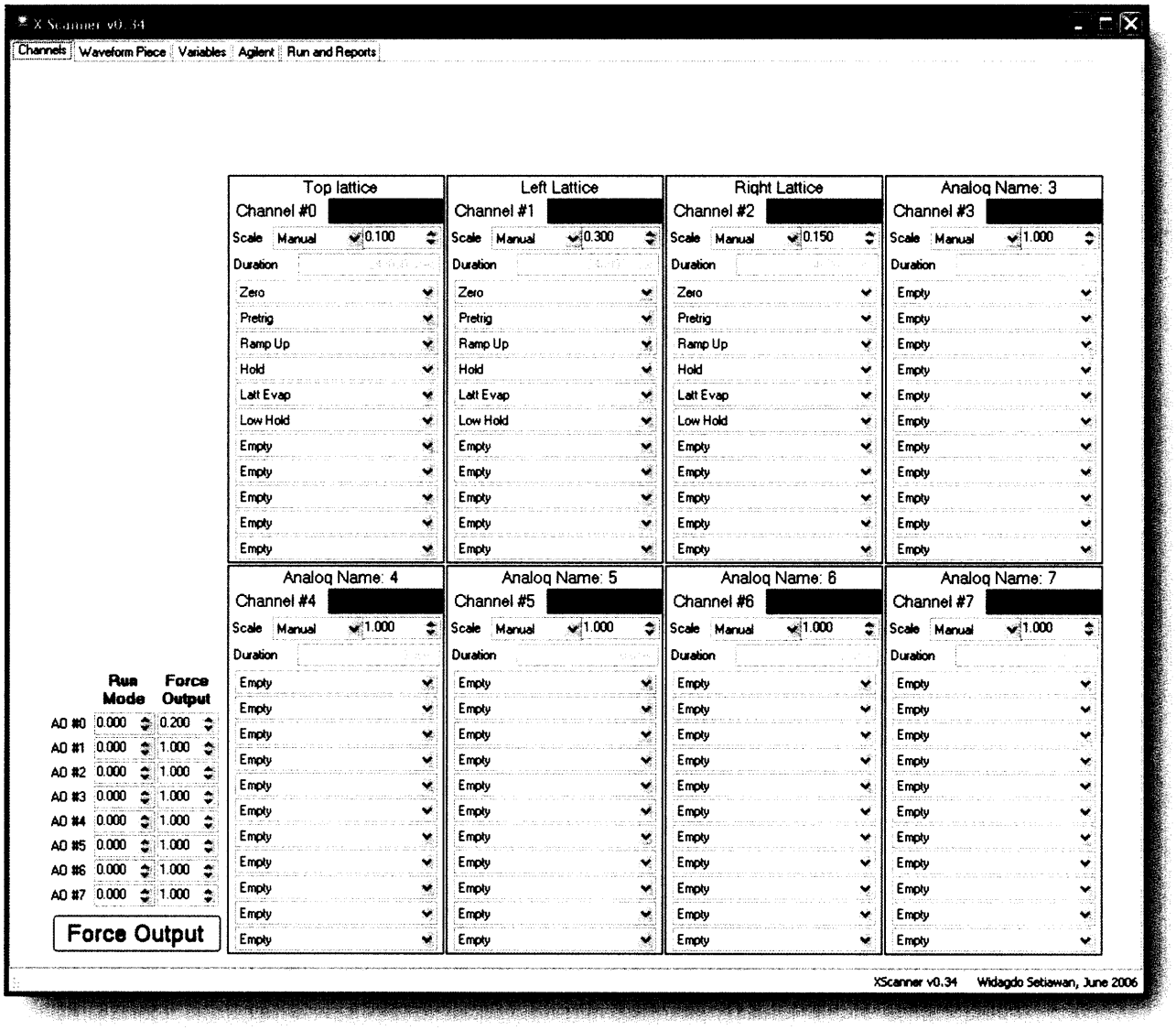

Figure C - 1. The main control of X Scanner.

The main control of X Scanner s is shown in Figure C - 1. For each channel, the user can select the available waveform to output in certain order. Furthermore, there is an overall scaling that is used to calibrate the lattice depth.

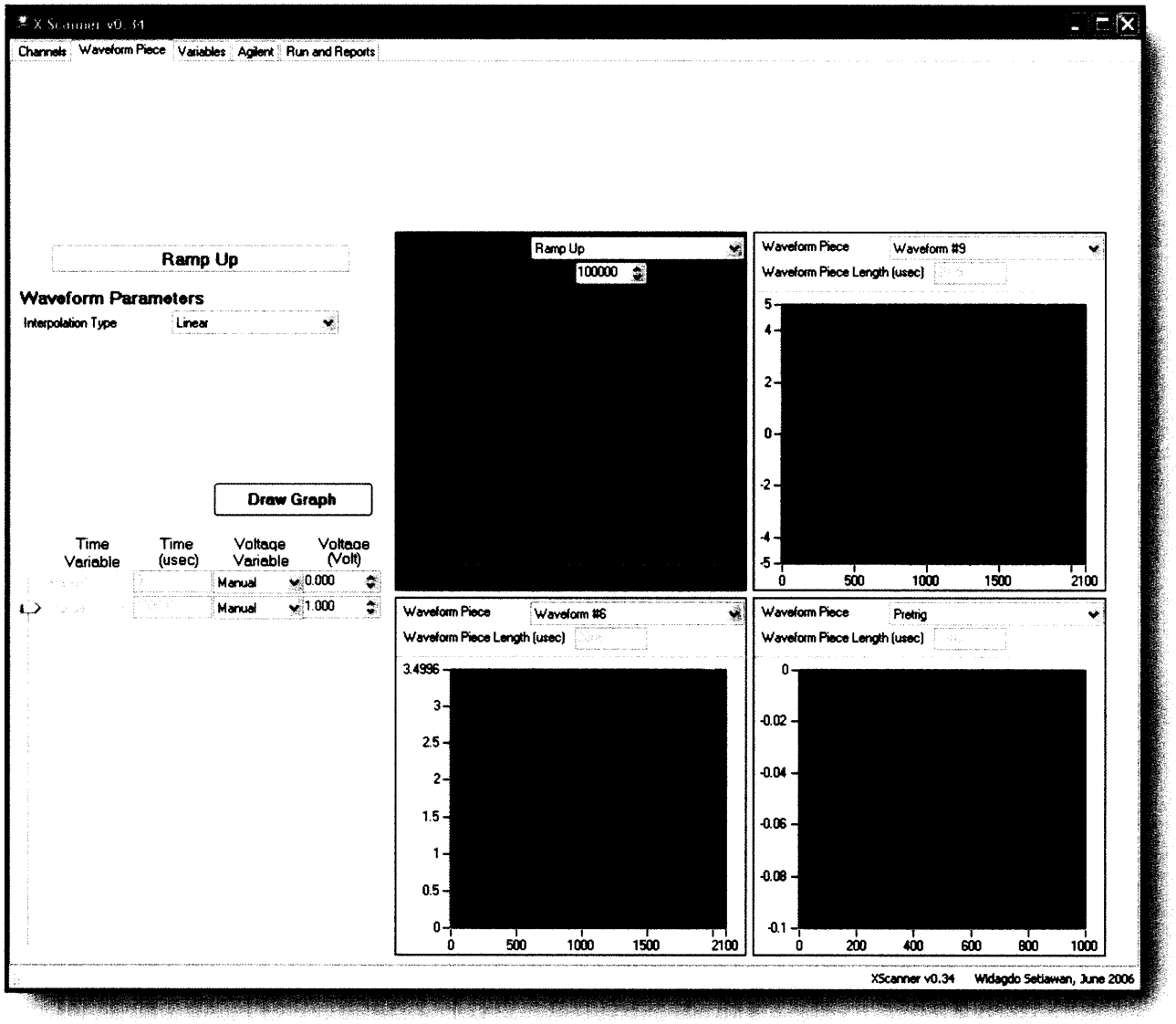

Figure C - 2. The waveform editor of X Scanner.

Figure C - 2 displays the waveform editor. The user can select from several possible interpolation such as linear, step, exponential, and sinusoidal. The sinusoidal interpolation is particularly useful when doing lattice depth modulation experiment.

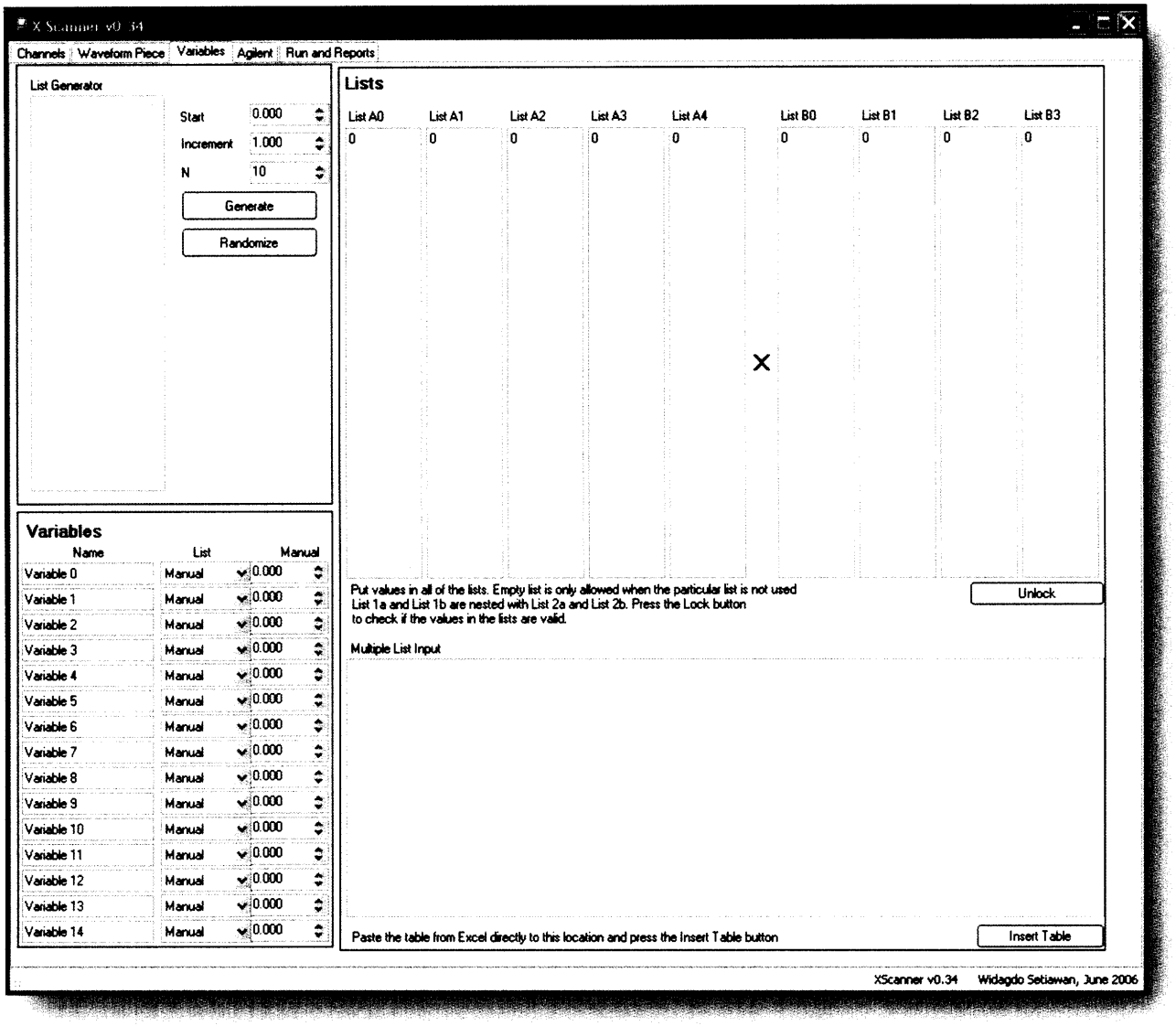

Figure C - 3. The automation feature of the X Scanner.

Figure C - 3 shows the automation feature of the X Scanner. The user can input a list of values to be run on the experiment. The program then goes through the list, changing its output depending on the current value. The user can generate the list using external software, such as Microsoft Excel, and import the lists to X Scanner.

C.4 Result

This program has been very successful in increasing the productivity of the lab especially in doing experiments that require a lot of data. Writing the software also gave me enough experience to do a more ambitious goal of rewriting the old Word Generator.

D IPG Laser Controller

D.1 Introduction

Our experiment has the capability to trap atoms or molecules using an Optical Dipole Trap (ODT). We use a YAG laser from IPG Photonics [7] shown in Figure D - 1. The laser model is YLR LP-SF 20 watt, single frequency, single mode PM fiber delivery laser system. The same laser is also used to create the optical lattices.

Figure D - 1. IPG Laser. Image is taken from the IPG website [7]

The power of the laser is determined by the current of the laser. In order to reach the desired power, user has to increase the current at the laser slowly (in 5 to 10 minutes) as the laser stabilizes. Rather than increasing the current manually, we ramp the current automatically using a computer via the serial port connector at the laser.

D.2 Software

The snapshot of the software can be seen in Figure D - 2. As usual, the software is written in C# from Microsoft Visual Studio 2005. User can select the desired current, and the software will automatically ramp the current of the laser slowly. This software saves about 20 minutes of our time every day. The software also reduces the possibility of human error since we do not have to ramp the laser current manually anymore.

The software also monitors other laser parameters such as the back reflection, interlock, temperature, and emission of the master laser as can be seen in Figure D - 2.

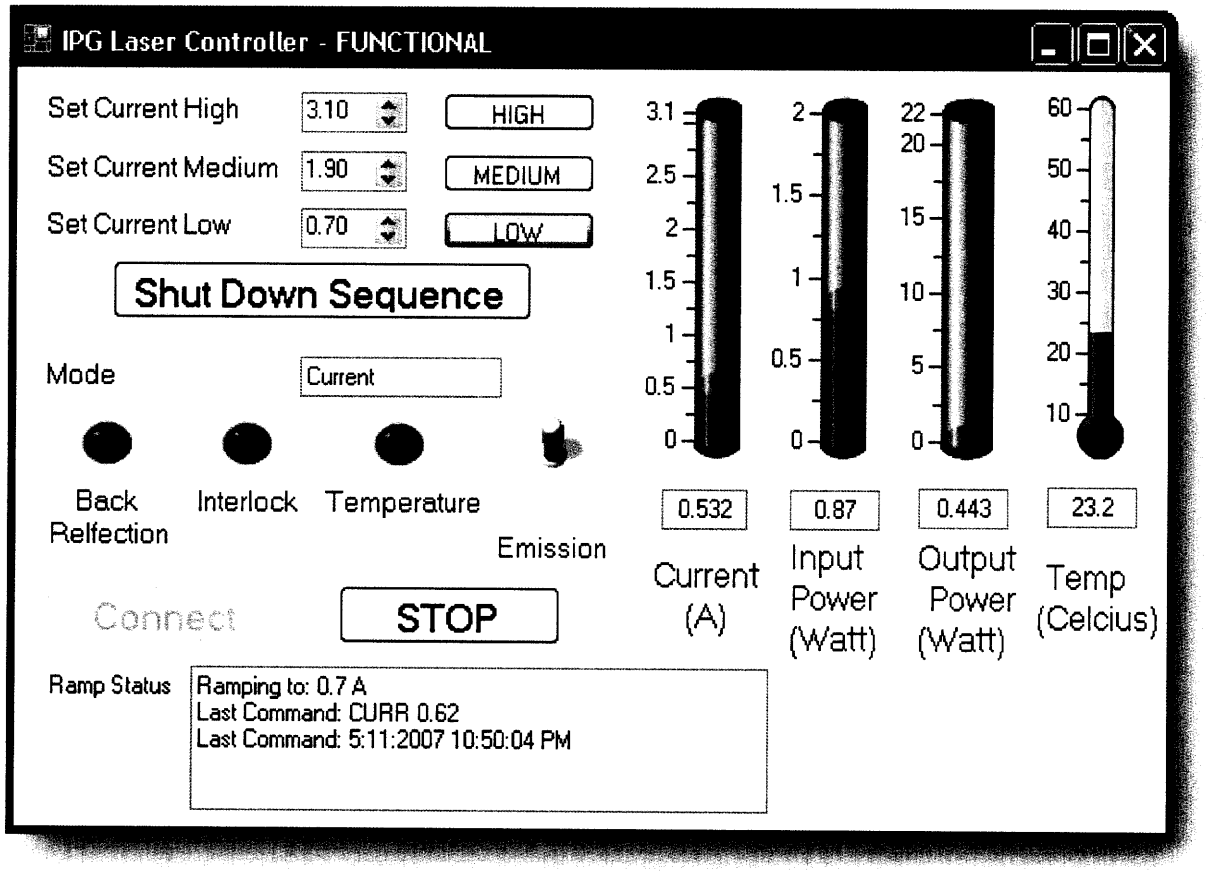

Figure D - 2. IPG Laser Controller.

Bibliography

1. *Laser Cooling and Trapping of Neutral Atoms.* **Phillips, W. D.** 70, 1998, Review of Modern Physics.
2. *High-Temperature Superfluidity of Fermionic Atoms in Optical Lattices.* **W. Hofstetter, J. I. Cirac, P. Zoller, E. Demler, M. D. Lukin.** 22, s.l. : Physical Review Letter, 2002, Vol. 89.
3. *Many-Body Physics with Ultracold Gases.* **Immanuel Bloch, Jean Dalibard, Wilhelm Zwerger.** s.l. : arXiv, 2007.
4. *Evidence for Superfluidity of Ultracold Fermions in an Optical Lattice.* **J. K. Chin, D. E. Miller, Y. Liu, C. Stan, W. Setiawan, C. Sanner, K. Xu, W. Ketterle.** s.l. : Nature, 2006, Vol. 443.
5. **Zwierlein, Martin.** *Cooling and Trapping a Bose-Fermi Mixture of Dilute Atomic Gas.* Cambridge : Thesis, 2001. Vol. Thesis.
6. TA 100. *TOPTICA Photonics.* [Online] http://www.toptica.com/page/Amplified_Tunable_Single_Mode_Diode_Laser_TA100.php?menu=132.
7. *Practical Uses and Applications of Electro-Optic Modulators.* **New Focus.** Application Note.
8. *Electrooptic properties of lithium niobate crystals for extremely high external electric fields.* **M. Luennemann, U. Hartwig, G. Panotopoulos, K. Buse.** 2003, Applied Physics B, pp. 403-406.
9. **Chuang, Isaac.** Modeling the NMR Probe. *Junior Lab Experimental Guide.*
10. *Frequency-modulation spectroscopy: a new method for measuring weak absorptions and dispersions.* **Bjorklund, Gary C.** 1, s.l. : Optical Society of America, January 1980, Optics Letters, Vol. 5, p. 15.
11. Pixelfly Double Shutter. *PCO Imaging.* [Online] http://www.pco.de/pco/php/products/index_1-en__01030401&view=detail&cam=47.html.
12. IPG Photonics. [Online] 2007. http://www.ipgphotonics.com/products_1micron_lasers_singlefrequency_ylr-lp-sfs.htm.